https://doi.org/10.5194/cp-2023-23
Preprint. Discussion started: 27 April 2023

Climate of the Past Discussions

Evolution of winter precipitation in the Nile-River watershed since the last glacial

Vera D. Meyer[1*], Jürgen Pätzold[1], Gesine Mollenhauer[1,2], Enno Schefuß[1*]

[1]MARUM – Center for Environmental Sciences, University of Bremen, Bremen, 28359, Germany
[2]Alfred Wegener Institute, Helmholtz Centre for Polar and Marine Research, Bremerhaven, 27570, Germany

Correspondence to: Vera D. Meyer (vmeyer@marum.de), Enno Schefuß (eschefuss@marum.de)

Abstract. Between 11.5 and 5 ka BP, the Sahara was vegetated owing to a wet climate during the African Humid Period (AHP). However, the climatic factors sustaining the "Green Sahara" are still a matter of debate. Particularly the role of winter precipitation is poorly understood. Using the stable hydrogen isotopic composition (δD) of high molecular weight (HMW) *n*-alkanoic acids in a marine sediment core from the Eastern Mediterranean (EM), we provide a continuous record for winter precipitation in the Nile-River delta spanning the past 18 ka. Pairing the data with regional δD records from HMW *n*-alkanes, we show that HMW *n*-alkanoic acids constantly derive from the delta while the HMW *n*-alkanes also receive significant contributions from the headwaters between ~15-1 ka BP due to enhanced fluvial runoff. This enables us to reconstruct the evolution of Mediterranean (winter) and monsoonal (summer) rainfall in the Nile River watershed in parallel. Heinrich Stadial 1 (HS1) evolved in two phases with a dry spell between ~17.5-16.0 ka BP followed by wet conditions between ~16-14.5 ka BP owing to movements of the Atlantic storm track. Winter rainfall enhanced substantially between 11-6 ka BP lagging behind the intensification of the summer monsoon by ca. 3 ka. Heavy winter rainfall resulted from a southern position of the Atlantic storm track combined with elevated sea-surface temperatures in the EM reinforcing local cyclogenesis. We show that during the "Green Sahara" monsoon precipitation and Mediterranean winter rainfall were simultaneously enhanced and infer that the winter-rainfall zone extended southwards delivering moisture to the Sahara. Our findings corroborate recent hypotheses according to which southward extended winter rains were a crucial addition to the northward displacement of the summer monsoon helping to sustain a "Green Sahara".

1 Introduction

North Africa underwent dramatic oscillations between dry and wet climate states in the course of glacial-interglacial cycles (deMenocal et al., 2000a). The last wet phase, known as the "African Humid Period" (AHP), occurred between 14.5-5 ka BP reaching its climax between 11-6 ka BP (e.g. deMenocal et al., 2000a; Shannahan et al., 2015; Tierney et al., 2017). Humid conditions in North Africa transformed the formerly barren, hyperarid Sahara Desert into a fertile "Green Sahara" (~11.5-5 ka BP; Kuper and Kröpelin, 2006) where savannah, lakes, rivers and wetlands existed allowing human settlements in the Sahara (Kuper and Kröpelin, 2006; Quade et al., 2018; Larrasoña et al., 2013; Jolly et al., 1998). Although intensively studied, the

https://doi.org/10.5194/cp-2023-23
Preprint. Discussion started: 27 April 2023

drivers and spatio-temporal extent of the AHP are still a matter of debate (Lüning and Vahrenholt, 2019; Kutzbach et al., 2014; Otto-Bliesner et al., 2014; Menviel et al., 2021; Tierney et al., 2017; Sha et al., 2019; Cheddadi et al., 2021). There is consensus that the AHP initiated in response to insolation forcing which intensified the African summer monsoon and shifted the Intertropical Convergence Zone and the African rainbelt northward (Menviel et al., 2021; Lüning and Vahrenholt, 2019; Pausata et al., 2016; Braconnot et al., 2007; Claussen et al., 2017; deMenocal et al., 2006b). Next to orbital forcing positive, non-linear feedbacks from the land surface amplified the climatic changes (e.g. Chandan et al., 2020; Pausata et al., 2016; 2020). Controversy exists on the termination of the AHP (Kuper and Kröpelin, 2006; Shannahan et al., 2015; Schefuß et al., 2005; Costa et al, 2014; Blanchet et al., 2014; deMenocal et al., 2000a; Tierney and deMenocal, 2013; Ménot et al., 2020; Tierney et al., 2008; Berke et al., 2012; Weldeab et al., 2014; Junginger et al., 2014; Castañeda et al., 2016a; deMenocal, 2015; Collins et al., 2017) as well as on the climatic processes sustaining a vegetated Sahara (Cheddadi et al., 2021, Kutzbach et al., 2014; Alpert et al., 2006; Chandan et al., 2020; Braconnot et al., 2007; Hopcroft et al., 2017; Claussen et al., 2017; Sha et al., 2019; Tierney et al., 2017). Paleoclimate records suggest both a gradual as well as an abrupt ending of the AHP and indicate that the AHP terminated earlier in the North than in the South (Kuper and Kröpelin, 2006; Shannahan et al., 2015; deMenocal, 2015). For a long time, most studies focused on the northward extension of the summer monsoon seeking to explain the AHP and the Green Sahara (deMenocal et al., 2006b; Braconnot et al., 2007; Menviel et al., 2021; deMenocal et al., 2000b; Shannahan et al., 2015; Sha et al., 2019; Tierney et al., 2017). However, the comparison of simulations and vegetation reconstructions shows that climate models probably underestimate precipitation in the northern Sahara and that the summer monsoon alone may have been insufficient to sustain a vegetated Sahara (Chandan et al., 2020; Braconnot et al., 2007; Hopcroft et al., 2017; Perez-Sanz et al., 2014; Cheddadi et al., 2021; Hély et al., 2014). Recently, Cheddadi et al. (2021) suggested that intensified Mediterranean winter rainfall and a southward extension of the winter rainfall zone into the Sahara may have delivered the additional moisture needed for sustaining a Green Sahara by decreasing rainfall seasonality. Also, Tierney et al. (2017) have already invoked additional winter precipitation to fully explain their observed amplitudes in precipitation change in Northwest Africa. Unfortunately, the glacial-to-Holocene development of winter precipitation in northeast Africa remains elusive given the scarcity of proxy records. In order to improve the understanding of how winter and summer precipitation evolved around the AHP, continuous records for precipitation are required to robustly investigate spatial variations in rainfall across North Africa.

A key region to study Northeast-African climate change is the Nile-River basin which - extending over 3 million km2 (Figure 1) - currently is influenced by monsoonal summer rains south of the Sahara Desert and Mediterranean winter rainfall in the delta region. Furthermore, it is of societal relevance to address the climatic history of the Nile River catchment because the river is the lifeline of Egypt providing fertile ground and drinking water to millions of people. It also played an important role in the rise and demise of ancient Egyptian civilizations (e.g. Zaki et al., 2021). Continuous archives for precipitation are predominantly found in the headwaters of the Nile River and further south (Lakes Victoria, Tana, Tanganyika; Berke et al., 2012; Costa et al., 2014; Tierney et al., 2008; 2010). In the northern part of the catchment where the hyperarid Sahara Desert extends, continuous records for precipitation are sparse as sedimentary sequences from the deglaciation and the Holocene -

such as lacustrine deposits - were subject to strong wind erosion during arid periods (Hamdan et al., 2016; Hamdan and Lucarini, 2013). Sediment cores from the Levantine Basin (Figure 1) have often been used to reconstruct environmental changes in the Nile-River watershed. These records are commonly considered as integrators of the entire catchment and are mostly interpreted to reflect monsoonal rainfall variability (Castañeda et al., 2016a; Revel et al., 2015; Ménot et al., 2020, Blanchet et al., 2014). However, the Nile crosses several climate regimes which drastically differ in precipitation amount and seasonality (tropical conditions in the headwaters, hyperarid desert in its central part and Mediterranean winter rainfall in the delta region). For climate reconstructions it is crucial to address these climate zones separately in order to identify latitudinal differences and to understand how monsoonal (summer) and Mediterranean (winter) precipitation evolved around the AHP.

Here, we provide a new hydroclimate record based on the stable hydrogen isotopic composition (δD) of HMW *n*-alkanoic acids. HMW *n*-alkanoic acids are major components of epicuticular leaf-waxes of higher plants (Eglinton and Hamilton, 1967). The record is obtained from marine sediment core GeoB7702-3 from the Eastern Mediterranean Sea (EM; Figure 1). δD of leaf-wax lipids (δD_{wax}) is a powerful means to reconstruct past hydrological changes (e.g. Sachse et al., 2012) and has been successfully applied to infer hydroclimate variability across Africa (Schefuß et al., 2005; Tierney et al., 2008; 2017; Berke et al., 2012; Costa et al., 2014; Collins et al., 2013; Castañeda et al., 2016a). We infer that δD_{wax} of our HMW *n*-alkanoic acids records winter precipitation in the Nile-delta region. By comparison to existing δD_{wax} records based on HMW *n*-alkanes from the Levantine Basin (Castañeda et al., 2016a) and HMW *n*-alkanoic-acid based δD_{wax} records from the headwaters (Berke et al., 2012; Costa et al., 2014; Tierney et al., 2008) we are able to address the individual hydroclimate developments of the southern and northern sections of the Nile-River catchment and shed light onto the interplay of Mediterranean (winter) and monsoonal (summer) rainfall changes in Northeast Africa around the AHP.

2 Study Area

Core GeoB7702-3 was recovered from the southeastern Levantine Basin off Israel (Figure 1) (Pätzold et al., 2003). The core receives terrigenous material from the Nile River as the Nile suspension load is transported eastward along the continental margin due to the anticlockwise direction of surface currents and eddies (e.g. Weldeab et al., 2002). This makes site GeoB7702-3 a suitable archive for environmental changes in the Nile-River basin (Castañeda et al., 2010; 2016).

The Nile River is the longest river in the world extending over 31° of latitude (Figure 1). The catchment spans from Equatorial Africa to the Mediterranean coast draining Uganda, Ethiopia, South Sudan, Sudan and Egypt (Figure 1). The river consists of three major tributaries, i.e. the White Nile (sourced from Lake Victoria), the Blue Nile (sourced from Lake Tana) and the Atbara Nile (source is situated north of Lake Tana). The confluence of the three tributaries forms the Main Nile (Figure 1). For the following discussion, we define three sub-catchments of the watershed as follows: upper catchment (headwaters in Ethiopia and Uganda; 0 to 15°N), middle catchment (Sahara, Sudan and Egypt; 15-30°N) and lower catchment (Nile delta; 30-31°N). On its way to the North the Nile River crosses different climate zones and vegetation regimes. The climate zones encompass Mediterranean climate in the delta area, the hyperarid Sahara Desert, the semiarid Sahel zone and a wet, tropical

https://doi.org/10.5194/cp-2023-23
Preprint. Discussion started: 27 April 2023

climate in Ethiopia and Uganda (e.g. Korecha and Barnston, 2007). In the lower and middle catchment, rainfall mainly occurs

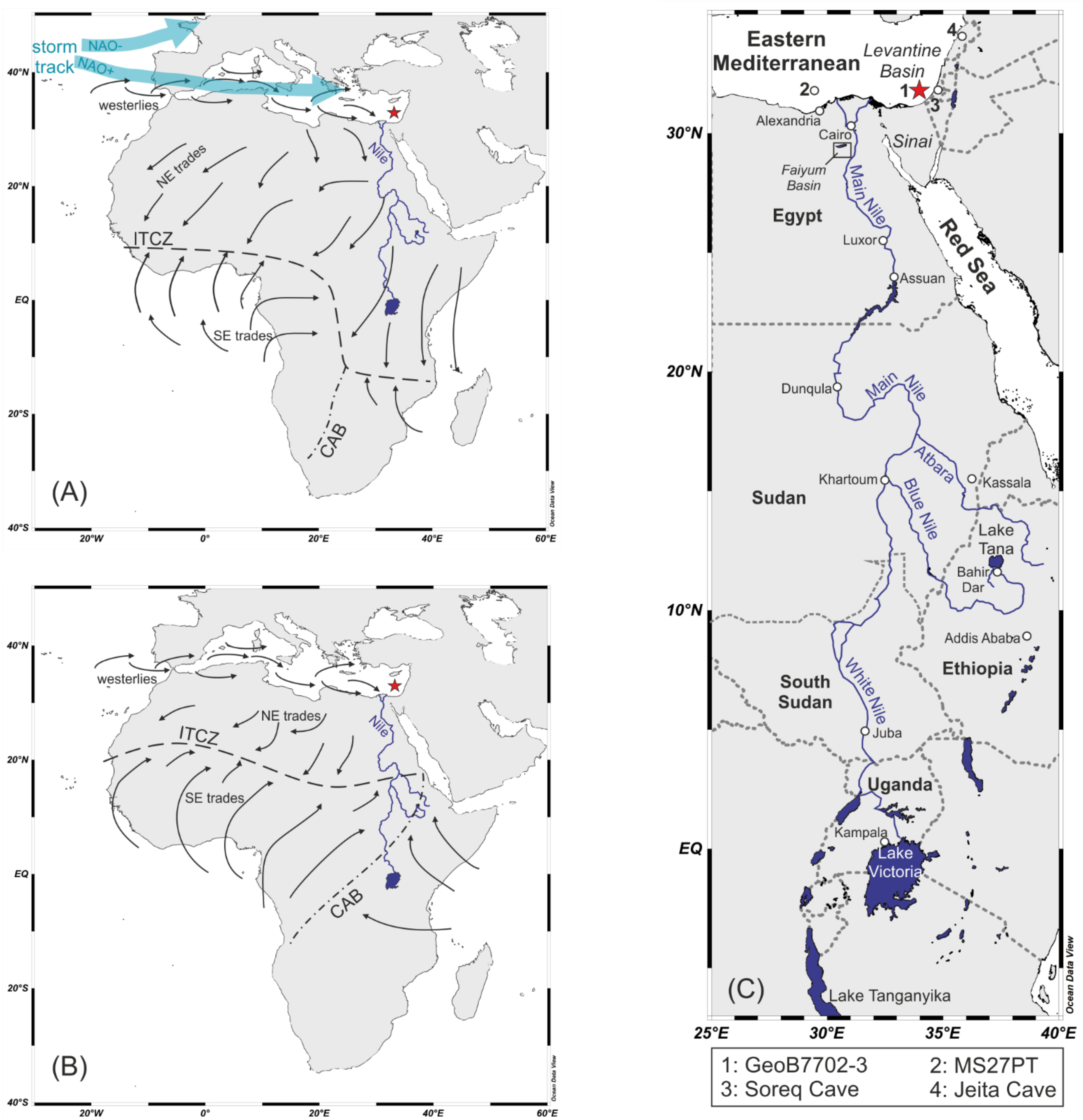

Figure 1: General wind patterns over Africa during winter (A) and summer (B). The star marks site GeoB7702-3. The modern positions of the ITCZ during January (A) and July/August (B) are illustrated. CAB means Congo Air Boundary which separates Atlantic and Indian air masses over equatorial Africa. In (A) the positions of the North Atlantic storm track are sketched for positive and negative phases of the North Atlantic Oscillation (NAO). (C) Detailed map of the Nile-River watershed. Site GeoB7702-3 is

https://doi.org/10.5194/cp-2023-23
Preprint. Discussion started: 27 April 2023

marked by a red star. Other locations mentioned in the text are indicated by circles. The maps were created using Ocean Data View 5.6.3 (Schlitzer, 2006).

during winter. In the Nile delta annual rainfall spans from 118 mm/yr at the coast (Alexandria; https://en.climate-data.org) to 18 mm/yr at its southern edge (Cairo; https://en.climate-data.org). Most rain falls between October and March. The Sahara usually does not receive any rainfall (e.g. Luxor; https://en.climate-data.org). The upper section of the watershed is characterized by heavy rainfall (e.g. about 1874 mm/yr annually in Addis Ababa/Ethiopia; about 1747 mm/yr in Kampala/Uganda; https://en.climate-data.org). In Ethiopia, most rain falls between June and September (https://en.climate-data.org). Uganda receives year-round precipitation with rainfall maxima during March till Mai and September till November (https://en.climate-data.org).

Precipitation in the upper Nile River watershed is mainly determined by the West African Monsoon, and thus related to the seasonal migration of the Intertropical Convergence Zone (ITCZ; Figure 1). During the summer months, the seasonal northward movement transports moisture-laden air to southern Northeast Africa (up to ~15°N). Additionally, the Congo Air Boundary controls the relative contribution of moisture from the Gulf of Guinea, i.e. the Atlantic Ocean, and Indian Ocean to the headwaters (Figure 1) (Camberlin, 2009). North of 15°N the catchment is predominantly under the influence of the westerlies receiving moisture from the Atlantic Ocean and the Mediterranean Sea, the Arabian Peninsula and the Red Sea (Figure 1) (Viste and Sortberg, 2013). The Mediterranean climate is characterized by dry summers and wet winters. The winter climate is largely dependent on the North Atlantic Oscillation (NAO) which forms a constituent of the Arctic Oscillation. Modulating the positions of the Atlantic and Mediterranean storm tracks (Figure 1) the NAO exerts strong control over moisture delivery to the Mediterranean borderlands. Warm and wet winters are generally associated with negative NAO-states while cold and dry winters occur during positive phases.

3 Material and Methods

3.1 Core Material and Chronology

Gravity core GeoB7702-3 was recovered from the continental slope off Israel at 562 m water depth during RV Meteor cruise M52/2 in 2002 (Pätzold et al., 2003). Prior to sampling the core was stored at 4°C. Age control for this core was previously established by Castañeda et al. (2010a) and is based on accelerator mass spectrometry (AMS) radiocarbon dates of planktic foraminifera. We refined the age model using up-to-date calibration curves and nine additional AMS dates (Table 1). To isolate foraminifera the samples were wet-sieved and specimens of the foraminifera Globigerinoides ruber alba were hand-picked from the (150-63 µm fraction). In cases where the abundance of G. ruber was insufficient, we mixed planktonic foraminifera species to obtain enough material (Table 1). 290-810 µg carbon was dated at the MICADAS AMS-dating facility at the Alfred Wegener Institute, Helmholtz Centre for Polar and Marine Research (Bremerhaven, Germany) according to inhouse protocols (Mollenhauer et al., 2021). The dates were combined with the data set of Castañeda et al. (2010a) to create the age-depth model. All radiocarbon dates are listed in Table 1. The BACON 2.5.8 software (Blaauw and Christen, 2011) was used for age-depth modeling. Radiocarbon ages were transferred into calendar ages based on the Marine20 calibration curve (Heaton et al., 2020). Today, the mean reservoir age offset (ΔR) in the Levantine Basin is -94 ±94yrs in relation to Marine20 at present (marine reservoir correction database; Reimer et al., 2001). BACON was run with a constant ΔR= -100 ±100yrs, accordingly. Default settings were used for the priors, apart from the accumulation prior, which was set to 50. BACON operated with 118 core-slices.

For biomarker analysis the core was sampled in 5-12 cm steps providing a mean temporal resolution of ~350 years between samples.

3.2 Lipid extraction and isotopic analysis

The lipid extraction and isotopic analysis were performed at MARUM (University of Bremen, Germany). The sediment samples were freeze-dried and afterwards homogenized using a mortar and pestle. The soluble organic matter was extracted from ~5 g of sediment using an Accelerated Solvent Extractor (ASE200). Extraction was performed with three cycles lasting 5 minutes each, using Dichloromethane: Methanol (9:1) at 100°C and 1000 psi. 19-Methyl-Arachidic Acid was added to the samples as internal standard prior to extraction. The total lipid extracts were saponified using potassium hydroxide (KOH). The fatty acids were methylated using methanol of known isotopic signature. The fatty-acid methyl esters (FAMEs) were cleaned by means of column chromatography. Columns consisted of 4 cm deactivated silica in a Pasteur pipette with 5 mm diameter. FAMEs were recovered using Dichloromethane:Hexane (2:1).

Isotope analysis of stable hydrogen (δD) was performed using gas chromatography coupled to isotope ratio mass spectrometry (GC-IRMS). We used a Thermo Trace GC coupled to a MAT253 MS. Isotope values were measured against calibrated reference gas (H2). Values are reported in per mil relative to the VSMOW standards. A standard mixture consisting of 16 n-alkanes was run every sixth sample in order to monitor the performance of the system. For the δD analysis the accuracy and precision (mean deviation from offline values and the respective relative standard deviation, RSD) were 2.2‰ and 3.0‰, respectively. The machine was operated only when the average absolute deviation from offline values was <5‰. The H+3 - factor was measured daily and was 5.6 ±0.1 throughout the measurement series. Replicate measurements of the samples yielded a standard deviation of 0.1-3.8‰ for δD. We report the δD-signatures of the n-$C_{26:0}$ and n-$C_{28:0}$ alkanoic acids as they turned out to be the most abundant homologues in our samples. The δD of the respective FAMEs were corrected for the bias introduced during the methylation process using isotope mass balance (hereafter $\delta D_{wax\ n\text{-alkanoic acid}}$). $\delta D_{wax\ n\text{-alkanoic acid}}$ was further corrected for deglacial changes in global ice-volume applying stacked data of oxygen isotopic compositions ($\delta^{18}O$) of benthic foraminifera (L04-stack; Lisiecki and Raymo, 2005).

Next to δD, we also analyzed the stable carbon isotopic composition of HMW n-alkanoic acids ($\delta^{13}C_{wax\ n\text{-alkanoic acids}}$) as described in the supplementary material (S1).

https://doi.org/10.5194/cp-2023-23
Preprint. Discussion started: 27 April 2023

Climate of the Past Discussions

Table 1: List of AMS-dates and corresponding calendar ages (cal. age) used to establish the revised age-depth model of GeoB7702-3. AMS dates were compiled from this study and Castañeda et al. (2010a; 2010b). Samples from this study were dated at the MICADAS-dating facility at Alfred Wegener Institute (Bremerhaven, Germany) while Castañeda et al. (2010a; 2010b) performed dating at the Leibnitz Laboratory for Radiometric Dating and Stable Isotope Research (University of Kiel, Germany). Our new age-depth model is based upon the median values of the calendar ages calculated.

Depth [cm]	Sample label	Dated material	AMS date [^{14}C a BP]	2σ [±]	Cal. age min [a BP]	Cal. age max [a BP]	Cal. age median [cal a BP]	Cal. age mean [cal a BP]	Reference of AMS date
0	set*	-	100*	10	64	124	98	97	this study
10	KIA25649	G. ruber and O. universa	245	30	123	415	221	231	Castañeda et al. (2010b)
64.5	KIA25648	G. ruber and G. sacculifer	1725	25	1086	1682	1342	1356	Castañeda et al. (2010b)
81.5-84.5	6279.2.1	G. ruber	2340	26	1615	2285	1929	1933	this study
102	KIA24619	G. ruber	2965	55	2288	2849	2580	2576	Castañeda et al. (2010b)
130-133	6281.1.1	G. ruber	3586	24	3113	3685	3400	3400	this study
132	KIA24617	G. ruber	3500	35	3189	3643	3413	3416	Castañeda et al. (2010b)
198-201	6277.2.1	G. ruber	5399	25	5353	6014	5697	5697	this study
210	KIA24616	G. ruber	5600	40	5764	6383	6036	6043	Castañeda et al. (2010b)
231-234	7307.1.1	G. ruber	7393	45	7242	8138	7724	7718	this study
242.5	KIA25646	G. ruber and G. sacculifer	7845	40	8023	8866	8327	8358	Castañeda et al. (2010b)
251-254	6280.1.1	G. ruber	9309	28	9015	10110	9663	9652	this study
257	KIA24613	G. ruber	9070	60	9564	10290	9934	9928	Castañeda et al. (2010b)
278-281	6276.2.1	mixed planktonic foraminifera	10144	34	11051	12047	11502	11508	this study
279	KIA24612	mixed planktonic foraminifera	10470	70	11128	11839	11457	11463	Castañeda et al. (2010b)
297-300	6275.2.1	G. ruber	11827	32	12688	13729	13215	13213	this study
310	KIA24611	mixed planktonic foraminifera	12580	80	13593	14509	14035	14037	Castañeda et al. (2010b)
356	KIA24609	G. ruber	14130	100	16073	16781	16432	16431	Castañeda et al. (2010b)
359-362	6274.2.1	G. ruber	14420	37	16264	17074	16666	16664	this study
391	KIA24608	G. ruber	15830	120	17610	18515	18036	18048	Castañeda et al. (2010b)
393-396	6262.2.1	G. ruber	15275	39	17690	18728	18151	18176	this study
452	KIA25652	G. ruber	18810	150	21025	22260	21750	21717	Castañeda et al. (2010b)
497	KIA24605	G. ruber	20660	180	23106	24215	23747	23716	Castañeda et al. (2010b)
540.5	KIA24604	G. ruber	21840	220	24579	25711	25192	25179	Castañeda et al. (2010b)
581.5	KIA25653	mixed planktonic foraminifera	22230	190	25715	27340	26397	26436	Castañeda et al. (2010b)

* the core-top age was defined as 100 calendar ages in order to guarantee BACON calculates positive dates for the depths above the first AMS-date (i.e. 10 cm).

https://doi.org/10.5194/cp-2023-23
Preprint. Discussion started: 27 April 2023

4. Results

$\delta D_{wax\ n\text{-alkanoic acid}}$ range between -104 and -153‰. The n-$C_{26:0}$ and n-$C_{28:0}$ alkanoic acids behave similar regarding δD-values and trends (Figure 2d; green and orange lines). In general, $\delta D_{wax\ n\text{-alkanoic acid}}$ is higher during the deglacial than during the Holocene (Figure 2d). Two episodes of remarkable changes in $\delta D_{wax\ n\text{-alkanoic acid}}$ are evident in the record, i.e. between ~17.5-14.5 ka BP and between ~11-6 ka BP. At 17.5 ka BP $\delta D_{wax\ n\text{-alkanoic acid}}$ rapidly increased and recorded maximal values at 17.0 ka BP. Afterwards $\delta D_{wax\ n\text{-alkanoic acid}}$ decreased again reaching values similar to the late Holocene between 16.0 and 14.5 ka BP. At 14.5 ka BP $\delta D_{wax\ n\text{-alkanoic acid}}$ slightly increased again and then remained relatively constant until a striking minimum between 10.0 -6.0 ka BP was registered which begins and terminates abruptly (where abruptly is defined as within a few hundred years). At this time HMW n-alkanoic acids got depleted by 34 ‰, relative to the values found at 12 ka BP (Figure 2d). After the minimum there was little variability throughout the late Holocene.

Castañeda et al. (2016a) investigated the hydroclimate development in the Nile River watershed using δD_{wax} of HMW n-alkanes (another leaf-wax lipid; $\delta D_{wax\ n\text{-alkanes}}$) in core GeoB7702-3 (Figure 2d, dark green line). Comparing our $\delta D_{wax\ n\text{-alkanoic acid}}$ with the δDwax n-alkanes reveals distinct discrepancies. While $\delta D_{wax\ n\text{-alkanoic acid}}$ and $\delta D_{wax\ n\text{-alkanes}}$ were similar during the periods between 18-14.5 ka BP and at 1 ka BP (Figure 2d) $\delta D_{wax\ n\text{-alkanes}}$ were more negative than $\delta D_{wax\ n\text{-alkanoic acid}}$ for most of the time (up to ~25 ‰). The offset results from different long-term developments. $\delta D_{wax\ n\text{-alkanoic acid}}$ was rather stable between 15-11 ka BP whereas $\delta D_{wax\ n\text{-alkanes}}$ progressively became more negative from 15 ka BP onwards. Likewise, constancy is found in $\delta D_{wax\ n\text{-alkanoic acid}}$ between 6 ka BP till present while $\delta D_{wax\ n\text{-alkanes}}$ progressively increased throughout this period (Figure 2d). Both records agree with respect to the maximum at ~17 ka BP and the minimum between 10-7 ka BP (Figure 2d).

5. Discussion

δD_{wax} is dependent to the δD of the source water taken up by the plant during biosynthesis and thus can be used as tracer for δD of precipitation (e.g. Sachse et al., 2012). This, in turn, varies along with hydrological processes including rainfall amount, evapotranspiration and moisture source but also temperature changes affect the isotopic composition (Sachse et al., 2012). In low latitude regions δD_{wax} is predominantly influenced by rainfall amount (amount effect) as temperature effects are negligible (Sachse et al., 2012). This makes δD_{wax} a powerful tool to reconstruct glacial-interglacial fluctuations in rainfall amount and moisture source across Africa (Schefuß et al., 2005; Tierney et al., 2008; Berke et al., 2012; Costa et al., 2014; Collins et al., 2013; Castañeda et al., 2016a). However, changes in the relative abundance of C3 versus C4 plants may also overprint the hydrological signal in δDwax owing to different fractionation factors in the Calvin and Hatch-Slack photosynthetic pathways (e.g. Sachse et al., 2012). The δ13C signature of leaf wax lipids such as HMW n-alkanoic acids (δ13Cwax n-alkanoic acids) is a common means to asses past changes in the relative contributions of C3 versus C4 plants in the catchment (Sachse et al., 2012; Collins et al., 2013) and to evaluate potential impacts of vegetation changes on δD_{wax} (e.g. Castañeda et al., 2016a). In order to explore potential effects of vegetation changes on our $\delta D_{wax\ n\text{-alkanoic acid}}$ we correlate $\delta D_{wax\ n\text{-alkanoic acid}}$ and $\delta^{13}C_{wax\ n\text{-}}$

https://doi.org/10.5194/cp-2023-23
Preprint. Discussion started: 27 April 2023

alkanoic acids (Figure S1). Considering that the linear correlation yields low correlation coefficients (R2 < 0.5; supplementary Figures S1 and S2) the impact of vegetation changes on $\delta D_{wax\ n\text{-alkanoic acid}}$ is considered minor and hydrologic variations exerted dominant control on $\delta D_{wax\ n\text{-alkanoic acid}}$. Hence, we conclude that $\delta D_{wax\ n\text{-alkanoic acid}}$ is a robust proxy for changes in rainfall and moisture source in the Nile River watershed throughout the past 18 ka. In order to deduce deglacial changes in hydroclimate in the Nile-River catchment, we pair our $\delta D_{wax\ n\text{-alkanoic acid}}$ with the $\delta D_{wax\ n\text{-alkanes}}$ from Castañeda et al. (2016a). $\delta D_{wax\ n\text{-alkanes}}$ has been interpreted to reflect rainfall variability in the Nile-River watershed associated with changes in the African summer monsoon (Castañeda et al., 2016a). The fact that $\delta D_{wax\ n\text{-alkanoic acid}}$ and $\delta D_{wax\ n\text{-alkanes}}$ show dissimilar patterns in in the long-term trends suggests that the compounds recorded different hydrological developments which in turn implies that HMW *n*-alkanoic acids and HMW *n*-alkanes derived from different source areas. This conclusion seems reasonable considering that the Nile-River watershed extends over several climate zones and covers strong hydrological contrasts (tropical to subtropical and hyperarid desert). These zones are influenced by different atmospheric circulation patterns with the westerlies influencing the middle and lower catchments and the African monsoon controlling precipitation in the headwaters. Hence, the paired application of $\delta D_{wax\ n\text{-alkanoic acid}}$ and $\delta D_{wax\ n\text{-alkanes}}$ has the potential to reconstruct monsoonal along with westerly precipitation in the Nile River watershed. In order to understand the hydrologic signals recorded in $\delta D_{wax\ n\text{-alkanoic acid}}$ and $\delta D_{wax\ n\text{-alkanes}}$ it is crucial to investigate from which section of the watershed HMW *n*-alkanoic acids and HMW *n*-alkanes derive.

5.1 Sources areas of leaf-wax lipids in the Nile-River watershed

Leaf-wax based records from off river mouths often are interpreted as catchment integrating signals (e.g. Blanchet et al., 2014; Häggi et al., 2016; Hemmingway et al., 2016), as also done by Castañeda et al. (2016a) with respect to $\delta D_{wax\ n\text{-alkanes}}$ in core GeoB7702-3. However, several studies indicate that this does not generally hold true for all types of lipids and not for all river systems (Hemmingway et al., 2016; Agrawal et al., 2014; Galy et al., 2011). It has been reported that leaf-wax lipids may be representative only for specific parts of a river catchment and source regions may vary between compound-classes and even between homologues within a compound class (e.g. Hemmingway et al., 2016; Agrawal et al., 2014). Hemmingway et al. (2016) found that HMW *n*-alkanoic acids originate from a local source in the Congo River watershed while HMW n-alkanes serve as catchment wide integrator. The differences between $\delta D_{wax\ n\text{-alkanoic acid}}$ and $\delta D_{wax\ n\text{-alkanes}}$ found in GeoB7702-3 strongly imply that the two lipid types derive from different source areas in the Nile River watershed, at least for times when records of $\delta D_{wax\ n\text{-alkanoic acid}}$ s and $\delta D_{wax\ n\text{-alkanes}}$ diverge (i.e between 14.5-1 ka BP). Similar $\delta D_{wax\ n\text{-alkanoic acid}}$ and $\delta D_{wax\ n\text{-alkanes}}$ are found before 15 ka BP and from 1 ka BP onwards (Figure 2d) suggesting that the compounds derived from the same area at these times. In order to identify the source areas of HMW *n*-alkanes and HMW *n*-alkanoic acids in GeoB7702-3 at present, we converted the δD_{wax} values into δD values of precipitation corrected for vegetation changes and ice volume change ($\delta D_{p\text{-vc-ic}}$)

https://doi.org/10.5194/cp-2023-23
Preprint. Discussion started: 27 April 2023

according to the methods described in the supplementary material.

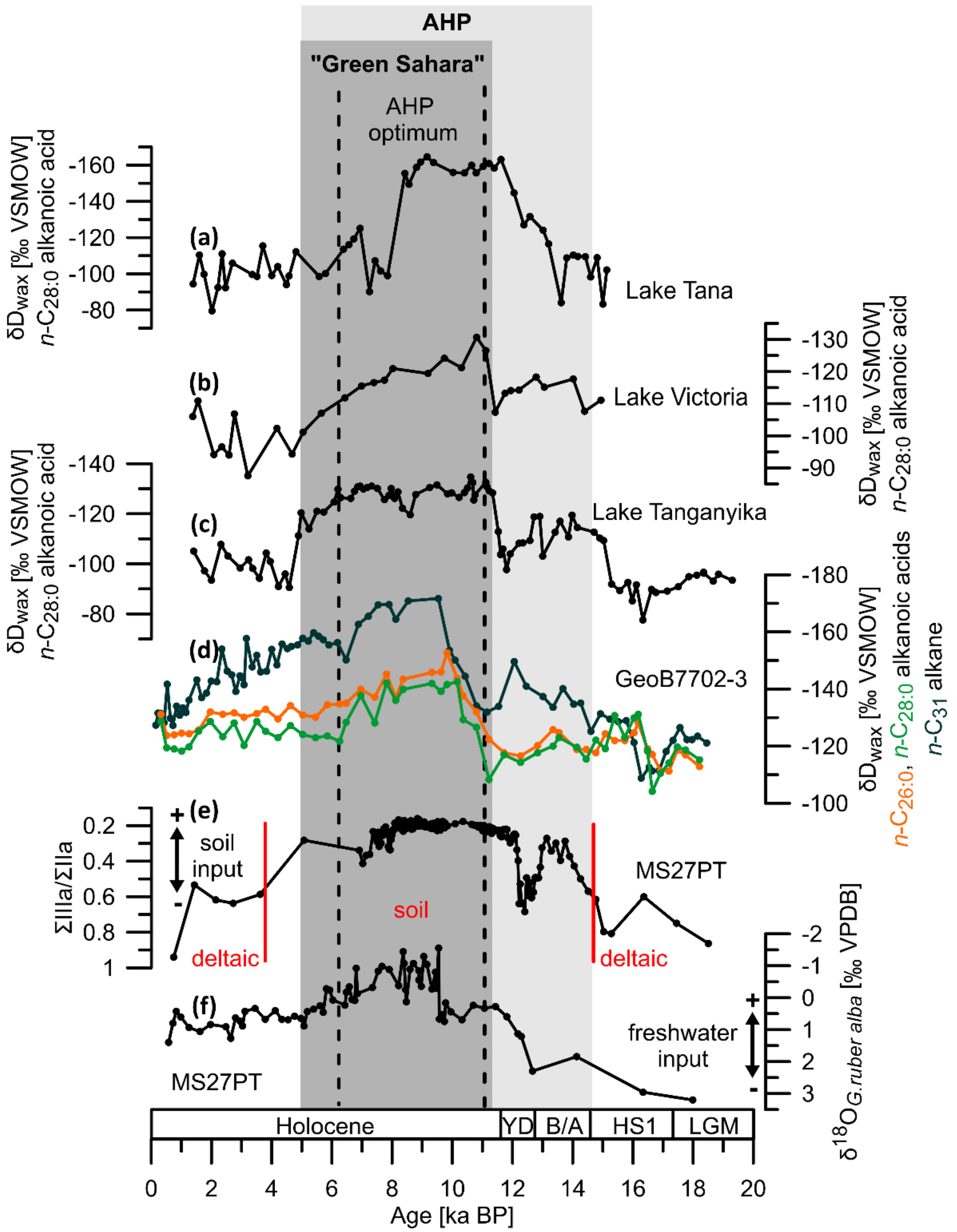

Figure 2: (a)-(c) δD$_{wax}$ records from Lakes Tana (Costa et al., 2014), Victoria (Berke et al., 2012) and Tanganyika (Tierney et al., 2008) reporting hydroclimate variability in tropical East Africa; (d) δD$_{wax\ n\text{-alkanoic acids}}$ (orange: *n*-C$_{26:0}$; green: *n*-C$_{28:0}$; this study) along with δD$_{wax\ n\text{-alkane}}$ (dark green: *n*-C$_{31}$; Castañeda et al., 2016a; 2016b) from core GeoB7702-3; (e) Ratio of tetra and penta-methylated brGDGTs from the Nile-deep sea fan (core MS27PT; Figure 1) reporting on the input of delta-derived organic matter versus material from the soils in the upper Nile-River catchment to the Eastern Mediterranean (Ménot et al., 2020); (f) oxygen

https://doi.org/10.5194/cp-2023-23
Preprint. Discussion started: 27 April 2023

isotopic composition of the planktic foraminifera species *Globigerinoides ruber alba* from the Levantine Basin (core MS27PT; Figure 1) used to reconstruct changes in salinity related to Nile River runoff (Revel et al., 2010; 2015). The light grey and dark grey shadings mark the episodes of the AHP and the Green Sahara, respectively. Dashed lines indicate the optimum of the AHP.

We compare the core-top values (here 15cm bsf translating into 0.31 ka BP) to mean weighted δD values of precipitation of the growing season ($\delta D_{p\text{-}gs}$) in the Nile catchment (Bowen et al., 2005). Bowen et al. (2005) define the growing season as months with mean temperatures >0°C. According to this definition, the values reported for the Nile River watershed are monthly weighted annual means since mean temperatures never drop below 0°C (https://en.climate-data.org). $\delta D_{p\text{-}gs}$ values from different parts of the catchment and the results from our $\delta D_{p\text{-}vc\text{-}ic}$ are listed in Table 2. The results downcore are given in Figure S3. For the core top $\delta D_{p\text{-}vc\text{-}ic}$ is around -14 ‰ for the *n*-C_{31} alkane and is -11 ‰ and -8 ‰ for the *n*-$C_{26:0}$ and *n*-$C_{28:0}$ alkanoic acids, respectively. This matches the isotopic composition of the Nile Delta where the predicted $\delta D_{p\text{-}gs}$ range between -15 and -11 ‰ (at Cairo, 30°3´N and Alexandria, 31°13´N; Bowen et al., 2005). Today, the Nile-Delta region receives the most deuterium-depleted precipitation in the entire watershed (Table 2; Bowen et al., 2005). In the middle section of the catchment, along the main Nile (30°N-15°N), $\delta D_{p\text{-}gs}$ becomes progressively more enriched towards the South (-4 ‰ at Assuan, 24°6´N and 10 ‰ in Khartoum, 15°35´N). In the headwater region, precipitation is more depleted compared to the Main-Nile but still is enriched by 10-17 ‰ (3.5 ‰ Lake Tana, 12°N and -5.6 ‰ Lake Victoria, 1°S; Table 2) relative to $\delta D_{p\text{-}gs}$ in the delta (Bowen et al., 2005). As such, we infer that HMW *n*-alkanoic acids and HMW *n*-alkanes predominantly derive from the delta region at present.

Table 2: Results for $\delta D_{p\text{-}vc\text{-}ic}$ calculated based on δD_{wax} for GeoB7702-3 at 15cm depth (~0.3 ka BP) together with $\delta D_{p\text{-}gs}$ values across the Nile River watershed. Locations listed are indicated in Figure 1.

Location	$\delta D_{p\text{-}vc\text{-}ic}$ [‰]	$\delta D_{p\text{-}gs}$[1] [‰]
GeoB7702-3; 15cm; C_{31} *n*-alkane	-14.87 ± 4.95	
GeoB7702-3; 15cm; $C_{26:0}$ *n*-alkanoic acid	-11.10 ± 3.14	
GeoB7702-3; 15cm; $C_{28:0}$ *n*-alkanoic acid	-8.78 ± 2.51	
Cairo/Nile Delta		-14.6 to -11.4
Alexandria/Nile Delta		-13.1
Assuan/Main Nile		-4.4
Dunqula/Main Nile		4.5 to 5.3
Khartoum/Main Nile		9.9
Kassala/Atbara		13.4 to 9.7
Bahir Dar/Lake Tana		3.5
Juba/White Nile		5.9
Kampala /Lake Victoria		-5.6

[1]: adopted from Bowen et al. (2005).

When comparing $\delta D_{wax\ n\text{-}alkanoic\ acid}$ and $\delta D_{wax\ n\text{-}alkanes}$ from GeoB7702-3 with $\delta D_{wax\ n\text{-}alkanoic\ acid}$ from Lakes in the headwater region and equatorial Africa (Lakes Tana, Victoria and Tanganyika (Figure 1); Berke et al., 2012, Tierney et al., 2008, Costa

https://doi.org/10.5194/cp-2023-23
Preprint. Discussion started: 27 April 2023

Climate of the Past
Discussions

et al., 2014) we find a strong similarity between long-term developments of $\delta D_{wax\ n\text{-alkanes}}$ and the lake records during the past 18 ka (Figure 2a, b, c, d). This suggests that $\delta D_{wax\ n\text{-alkanes}}$ records deglacial climate change in the headwaters of the river (Figure 2a, b, c, d) and that the source of the HMW *n*-alkanes must have changed at some point in the past. Accordingly, we propose that the HMW *n*-alkanes received substantial contributions from the headwater region between ~15-1 ka BP, the time when $\delta D_{wax\ n\text{-alkanoic acid}}$ and $\delta D_{wax\ n\text{-alkanes}}$ have dissimilar values. While the source of the HMW *n*-alkanes was dynamic during the past 18 ka, the source of the HMW *n*-alkanoic acids most likely was rather stable considering the dissimilar patterns in $\delta D_{wax\ n\text{-alkanoic acid}}$ from core GeoB7702-3 and the records from the lakes (Figure 2a, b, c, d). Considerable contributions of HMW *n*-alkanoic acids from the headwater region are unlikely. However, acknowledging that the Sahara was vegetated between ~11-5 ka BP (Kuper and Kröpelin, 2006) the source region of the HMW *n*-alkanoic acids may have extended further south into the northern Sahara at this time. Likewise, the HMW *n*-alkanes probably received additional contributions from the middle catchment of the river. During the AHP, site GeoB7702-3 may also have received additional material from the Sinai Peninsula through Wadi El Arish. This drainage basin is rather dry at present but got reactivated during the AHP (AbuBakr et al., 2013; Muhs et al., 2013).

Our scenario regarding dynamics in HMW *n*-alkane provenance fits findings from Ménot et al. (2020) who analyzed branched Glycerol Dialkyl Glycerol Tetraethers (brGDGTs) in the Nile deep sea fan in order to reconstruct soil input from the Nile River into the EM over the deglaciation. brGDGTs are synthesized by bacteria thriving in peat and soils (Weijers et al., 2006, Martin et al., 2019) but can also be produced in-situ in rivers and estuarine settings and in the marine sediments (deJonge et al., 2014). Using the ratio between tetra- and penta- methylated brGDGTs (ΣIIIa/ΣIIa-ratio) Ménot et al. (2020) inferred that the compounds derived from the Nile delta between 20-14.5 ka BP and after 4 ka BP (Figure 2e). The interval of soil-derived input (14.5-4 ka BP; Ménot et al., 2020) matches the interval of diverging $\delta D_{wax\ n\text{-alkanoic acid}}$ and $\delta D_{wax\ n\text{-alkanes}}$ (Figure 2d) during which considerable amounts of HMW *n*-alkanes from the upper and middle catchment were deposited in the EM sediments.

Being hydrophobic the HMW *n*-alkanes and HMW *n*-alkanoic acids are among the recalcitrant fraction of organic matter that is preserved for long times in the geological record and consequently is able to survive riverine transport and intermediate storage in reservoirs prior to burial in the marine sediments (e.g. Eglinton and Eglinton, 2008). However, our north-south allocation regarding the sources of HMW *n*-alkanoic acids and HMW *n*-alkanoic acids in GeoB7702-3 suggests that in the Nile-River watershed, the most of the HMW *n*-alkanoic acids sourced from the upper catchment did not reach site GeoB7702-3, most likely due to degradation during riverine transport. This is in accordance with findings from Hemmingway et al. (2016) who inferred that in the Congo-River catchment HMW *n*-alkanoic acids in suspended sediments from the outflow derive from local sources while HMW *n*-alkanes have a local and distal origin providing a more catchment integrated signal. Similarly, Agrawal et al. (2014) suggested that in the Ganga-Bahamaputra River system HMW *n*-alkanoic acids from the Himalayan headwaters degrade during transport and get replaced by HMW *n*-alkanoic acids from the local floodplains. There is consensus that HMW *n*-alkanoic acids are more prone towards degradation than HMW *n*-alkanes (Meyers and Ishiwatari, 1993; Hoefs et al., 2002; Sinninghe-Damsté et al., 2002; Galy and Eglinton, 2011; Hemmingway et al., 2016) which probably accounts for the discrepancies in provenance of HMW *n*-alkanoic acids and HMW *n*-alkanes observed in these large river systems (e.g. Hemmingway et al., 2016) and at our study site.

5.2 Environmental drivers of HMW *n*-alkane provenance

There is compelling evidence that during the early deglaciation and in particular Heinrich Stadial 1 (HS1) the Northeast African climate was very arid (Stager et al., 2011; Castañeda et al., 2016; Tierney et al., 2008; Tierney and deMenocal, 2013; Revel et al., 2014; Ménot et al., 2020). Lakes Tana and Victoria, the sources of the Blue and White Nile tributaries, desiccated between 17-16 ka BP (Stager et al., 2011; Lamb et al., 2007) leading to a drastic reduction in runoff in the Nile River system recorded by higher $\delta^{18}O$ values of the planktonic foraminifera species Globigerinoides ruber alba ($\delta^{18}O_{G.\ ruber\ alba}$; Figure 2f) offshore the Nile River mouth (Revel et al., 2010; 2015). The weak fluvial activity in the Nile River likely restricted the source of the leaf-wax lipids to the Nile delta. δD_{wax} records from Lake Tanganyika (Figure 2c) document that the East African climate became wetter around 14.5-15 ka BP (Tierney et al., 2008). In response to the wetter conditions the overflow of Lakes Tana and Victoria resumed around 15.5 and 14.5 ka BP (Williams et al., 2006; Marshall et al., 2011) and freshwater input from the Nile River increased accordingly as documented by lower $\delta^{18}O_{G.\ ruber\ alba}$ (Revel et al., 2010; 2014; 2015). The climate amelioration in Northeast Africa coincided with the onset of divergence between $\delta D_{wax\ n\text{-alkanes}}$ and $\delta D_{wax\ n\text{-alkanoic acid}}$ as well as with the switch to soil-derived brGDGTs (Figure 2). Enhanced fluvial energy in the headwaters probably increased erosion and export of organic matter in the upper reaches of the river. As mentioned above, a considerable amount of HMW *n*-alkanoic acids mobilized in the headwaters probably got degraded during riverine transport and did not reach the core site. During the late Holocene, at around 4 ka BP, drier conditions re-established in the headwaters and tropical East Africa (Tierney et al., 2008, Costa et al., 2014, Berke et al., 2012) and the Nile runoff reduced accordingly (Revel et al., 2015; 2010). Again, the delta became the predominant source of HMW *n*-alkanes and brGDGTs.

5.3 Hydroclimate development during the past 20 ka

As for the reconstruction of the hydroclimate variability our findings imply that the HMW *n*-alkanoic acids and the HMW *n*-alkanes can be used to reconstruct the hydroclimatic developments in the lower and upper reaches of the Nile River in parallel (between ~14.5-4 ka BP). As elaborated earlier, the delta is predominantly influenced by Mediterranean winter precipitation. According to our inference that the HMW n-alkanoic acids consistently derive from the delta $\delta D_{wax\ n\text{-alkanoic acid}}$ should record changes in winter precipitation throughout the past 18 ka. By contrast the $\delta D_{wax\ n\text{-alkanes}}$ should predominantly be a summer signal, as we infer that the HMW *n*-alkanes receive major contributions from the headwaters south of 15°N where the African summer monsoon controls precipitation. Given that the Sahara became vegetated during the Early Holocene, $\delta D_{wax\ n\text{-alkanes}}$ potentially also recorded changes in the middle catchment. The application of paired $\delta D_{wax\ n\text{-alkanes}}$ and $\delta D_{wax\ n\text{-alkanoic acid}}$ allows to investigate how westerly (winter) and monsoonal (summer) precipitation evolved around the AHP.

https://doi.org/10.5194/cp-2023-23
Preprint. Discussion started: 27 April 2023

5.4 early deglaciation – Heinrich Stadial 1 (18-14 ka BP)

Several authors pointed out that the LGM (21-19 ka BP) was a relatively moist interval in the southeast Mediterranean realm where conditions may have been similar to today (Wang et al., 2018). In the northeastern Sahara precipitation must have been sufficient to recharge aquifers from which tufa deposits formed in the Eastern Desert (Hamdan and Brook, 2015). During the LGM, the polar front and the westerlies were displaced to the south relative to today (situated at ca. 40°N; Wang et al., 2018) owing to the presence of the Fennoscandian ice sheet (Wang et al., 2018). Accordingly, storms frequently reached the Eastern Mediterranean and Northern Sahara providing the region with moisture (Hamdan and Brook, 2015; Wang et al., 2018). The Northeast African climate became harsher during the early deglaciation (from 19 ka onwards) and the most severe aridity occurred during HS1 (~18-14.5 kaBP; Tierney et al., 2008; Stager et al., 2008; Hamdan and Brook, 2015). Lakes Victoria and Tana desiccated (Berke et al., 2012; Costa et al., 2014) and in the eastern Sahara, tufa formation ceased (Hamdan and Brook, 2015). Also, in the Nile-River delta conditions may have rapidly become more arid at the beginning of HS1 given the abrupt increase of $\delta D_{wax\ n\text{-alkanoic acid}}$ as well as the $\delta D_{wax\ n\text{-alkanes}}$ (Castañeda et al., 2016) 17.8 ka BP (Figures 2d, 3d). Maximal values of $\delta D_{wax\ n\text{-alkanoic acid}}$ and $\delta D_{wax\ n\text{-alkanes}}$ suggest that also in the Nile River delta experienced the most arid conditions since the LGM at that time. However, the drought was restricted to the first half of HS1 and at ~16 ka BP, the climate rapidly transitioned into a wet phase that lasted until the end of HS1 (14.5 ka BP) (Figures 2d, 3d). Also, $\delta^{18}O$ of speleothems from the Soreq Cave/Israel suggest a progressive increase in precipitation at the same time (Figure 3b). $\delta D_{wax\ n\text{-alkanoic acid}}$ show that hydroclimatic conditions may have been similar to the late Holocene and today considering the similar values in δD (-130 to -125‰). The succession of dry and wet episodes within HS1 fits the growing view that HS1 evolved in two phases, the first one lasting from ~18.2- 16.2 ka and the second lasting from 16.2-14.5 ka BP (e.g. Naughton et al., 2023 and references within). Two-phase patterns with alternating dry and wet intervals have also been recorded by many marine and terrestrial archives in the entire Mediterranean realm (Valsecchi et al., 2012; Naughton et al., 2023; Naughton et al., 2009; 2016; Pérez-Mejías et al., 2021; Fletcher and Sanchez-Goñi et al., 2008). However, the records are inconsistent regarding the order of wet and dry episodes indicating a complex hydroclimate development in the Mediterranean borderlands throughout HS1. For example, the Sea of Marmara/Northeastern Mediterranean experienced wet conditions during the first phase of HS1 followed by drought during the second phase (Valsecchi et al., 2012). The opposite pattern is evident in our data at site GeoB7702-3. These regional differences are probably related to spatial variations of the Mediterranean storm track. Proxy-based and modeling studies suggest that the deglacial Mediterranean climate responded to abrupt climate fluctuations in the North Atlantic via atmospheric teleconnections involving the position of the westerly Jet and the associated storm track (Columbu et al., 2022; Valsecchi et al., 2012; Li et al., 2019). According to Li et al. (2019) a weakening of the Atlantic Meridional Overturning Circulation (AMOC) during HS1 would push the westerlies northward. Considering that during the LGM, the polar front and the westerlies were situated at ca. 40°N; (Wang et al., 2018) a northward movement of the westerlies and the Mediterranean storm track would explain why the climate became drier in the Nile River delta but concurrently wetter in the NE Mediterranean. A subsequent return to the South at ~16 ka BP would have reversed the situation with wet conditions in the Nile-River delta and

https://doi.org/10.5194/cp-2023-23
Preprint. Discussion started: 27 April 2023

concurrent aridity in the NE Mediterranean realm. Our inference agrees with findings from the western Mediterranean basin since Naughton et al. (2023) conclude that opposing successions of dry and wet phases on the Iberian Peninsula during HS1 document a northward followed by a southward movement of the polar front and the associated westerly Jet.

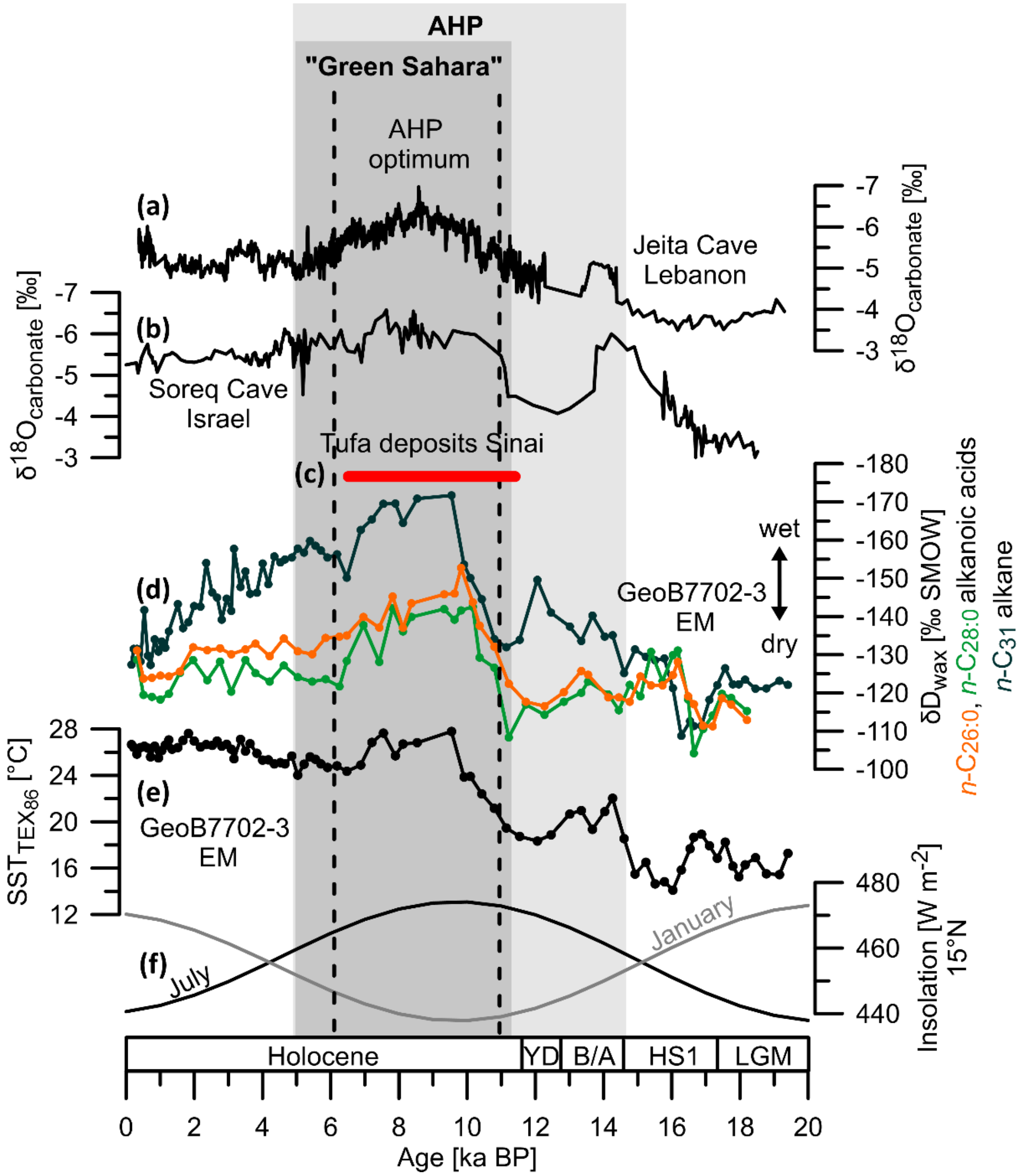

Figure 3: (a) Oxygen isotope records from speleothems ($\delta^{18}O_{carbonate}$) in Jeita Cave, Lebanon (Cheng et al., 2015); (b) Oxygen isotope records from speleothems in Soreq Cave, Israel (Bar-Mathews et al., 2003); (c) The red bar marks the interval during which spring-tufa deposits formed on the Sinai Peninsula (Hamdan and Brook, 2015); (d) $\delta D_{wax\ n\text{-alkanoic acids}}$ (orange: *n*-$C_{26:0}$; green: *n*-$C_{28:0}$; this study) along with $\delta D_{wax\ n\text{-alkane}}$ (dark green: *n*-C_{31}; Castañeda et al., 2016a; 2016b) from core GeoB7702-3; (e) sea surface temperature (SST) in the Eastern Mediterranean (EM) based on TEX_{86} from core GeoB7702-3 (Castañeda et al., 2010a; 2010c; 2016a); (f)

https://doi.org/10.5194/cp-2023-23
Preprint. Discussion started: 27 April 2023

Insolation during January and July at 15°N from Berger and Loutre (1991). The light grey and dark grey shadings indicate the episodes of the AHP and the Green Sahara, respectively. The AHP optimum is marked by dashed lines.

At the end of HS1, dry conditions established in the Nile-Delta region which suggests that the storm track moved north again. Relatively dry conditions prevailed in the Nile River delta until 11.5 ka BP as documented by $\delta D_{\text{wax } n\text{-alkanoic acid}}$ (Figure 3d) indicating that the storm frequency and westerly moisture supply must have remained weak in the region throughout this period. This contradicts records from the western, central and the NE Mediterranean region (e.g. Jeita Cave/Lebanon, Figure 3a) where wet episodes already occurred earlier coincident with the Bølling/Allerød (B/A) interstadial in the North Atlantic (Fletcher et al., 2010; Columbu et al., 2022; Valsecchi et al., 2012; Cheng et al., 2015). These are attributed to enhanced moisture delivery by stronger westerlies in the region (e.g. Columbu et al., 2022; Li et al., 2019). Also, subsequent reversals to drier conditions during the Younger Dryas (YD) have been identified (Fletcher et al., 2010; Columbu et al., 2022; Valsecchi et al., 2012; Cheng et al., 2015). These fluctuations are interpreted to document that the teleconnection between north Atlantic climate dynamics and Mediterranean rainfall via the westerly Jet mediated rainfall in the western, central and northeastern Mediterranean throughout the deglaciation (Columbu et al., 2022). The absence of such variations in the Nile River delta suggests that Atlantic climate forcing was suppressed in the northeastern Sahara. Once the Fennoscandian Ice Sheet retreated the polar front and the westerly Jet moved northwards (Wang et al., 2018) and probably pushed the trajectory of storms northwards accordingly leading to dry conditions in Nile River delta throughout the B/A and YD. Consequently, dynamics of the westerlies associated with AMOC-variations probably did not influence the Nile-River delta anymore. Considering that Jeita Cave recorded a wet interval during the B/A (Cheng et al., 2015; Figure 3a), the southern boundary of the storm track was probably situated between ~31-33°N at this time.

5.5 African Humid Period (14.5-5 ka BP)

Whereas $\delta D_{\text{wax } n\text{-alkanoic acid}}$ indicate relatively constant dryness after HS1, $\delta D_{\text{wax } n\text{-alkanes}}$ document a progressive depletion of plant waxes. As previously elaborated by Castañeda et al. (2016a), this progressive depletion starting at ~15 ka BP most likely stems from increasing rainfall amount in the headwaters of the Nile-River catchment. This development agrees with increasing humid conditions at Lake Tanganyika, Tana and Victoria and has been interpreted as intensification of the African summer monsoon (Castañeda et al., 2016, Berke et al., 2012; Tierney et al., 2008; Costa et al., 2014). This hydroclimate amelioration led into in the AHP which lasted from ~14.5-5 ka BP and culminated between ~11-6 ka BP (e.g. deMenocal et al., 2006a). More negative $\delta D_{\text{wax } n\text{-alkanoic acid}}$ may indicate that also the Nile Delta received substantially more rainfall during the AHP optimum, i.e. between 11.0-6.0 ka BP (Figure 2d). A case study conducted by Breitenbach et al., (2010) in the Bay of Bengal/Indian Ocean shows that intensified river discharge due to heavy summer-monsoon rainfall leads to surface water freshening in the Ocean which in turn lowers the δD-signature of precipitation derived from these surface waters. Considering that the $\delta^{18}O_{G.\ ruber\ alba}$ records from the Mediterranean Sea (Emeis et al., 2000; Revel et al., 2010; 2015) show massive surface freshening during the AHP, this effect could have potentially accounted for depleted $\delta D_{\text{wax } n\text{-alkanoic acid}}$ in addition to or instead of the amount effect. However, given that the $\delta^{18}O_{G.\ ruber\ alba}$ (Revel et al., 2010; 2015) and $\delta D_{\text{wax } n\text{-alkanoic acid}}$ show different

https://doi.org/10.5194/cp-2023-23
Preprint. Discussion started: 27 April 2023

temporal trends (Figure 2d,f) freshening of the Mediterranean probably constitutes only a minor part of the signal in $\delta D_{wax\ n\text{-}alkanoic\ acid}$. Therefore, the minimum in $\delta D_{wax\ n\text{-}alkanoic\ acid}$ most likely attests to drastically increased rainfall amount in the Nile River delta during the AHP. It is well constrained that the ITCZ shifted northward during the AHP supplying the Sahara with regular rainfall (e.g. deMenocal et al., 2006b; Menviel et al., 2021; Braconnot et al., 2007; Blanchet et al., 2021; Tierney et al., 2017; Kuper and Kröpelin, 2006; Hamdan and Brook, 2015). Some studies suggest that the monsoon fringe even expanded up to 31°N (Sha et al., 2019; Tierney et al., 2017) which would mean that the Nile-River delta (situated at 30-31°N; Figure 1) became influenced by the African summer monsoon. However, in most climate simulations the northernmost position of the ITCZ is located at ~24°N (e.g. Pausata et al., 2016) which is also corroborated by proxy data (Hamdan and Brook, 2015; Cheddadi et al., 2021). Thus, we consider it unlikely that the northward migration of the monsoon rainbelt caused the increased rainfall in the delta region. Instead, increased winter precipitation associated with the westerlies most likely was responsible for the minimum in $\delta D_{wax\ n\text{-}alkanoic\ acid}$.

5.5.1 Controls on enhanced winter precipitation

The rapid switch to wetter conditions at 11 ka BP as well as the abrupt return to dry conditions at 6.5 ka BP displayed by the $\delta D_{wax\ n\text{-}alkanoic\ acid}$ occurred congruently with a warm spell in the EM between 10-7 ka BP documented by the TEX_{86}-SST proxy from GeoB7702-3 (Castañeda et al., 2010a). The warm SST would have enhanced evaporation and local cyclogenesis over the Levantine Basin which in turn would have increased precipitation over the Nile-delta region. Records from the Middle East (Figure 3a,b), southern Europe and northwest Africa provide evidence that mild and wet conditions were widespread across the Mediterranean borderlands during the early Holocene (Cheddadi et al., 2021, Wagner et al., 2019, Bar-Mathews et al., 2003; Cheng et al., 2015). Today, relatively mild and wet winters in the Mediterranean realm are associated with negative phases of the NAO-Index during which the westerlies weaken and the Atlantic storm track is situated south steering Atlantic moisture and storms frequently into the Mediterranean (Figure 1). As invoked by several data- as well as model-based studies, negative NAO-like circulation patterns probably prevailed during the early Holocene promoting intense winter precipitation in the Mediterranean borderlands (Kutzbach et al., 2014, Arz et al., 2003, Dixit et al., 2020, Wassenburg et al., 2016). Previous work suggests that the southward displacement of the westerlies and the associated storm trajectory was a response to decreasing Northern Hemisphere winter insolation and thus a result of precessional forcing (Kutzbach et al., 2014; Wagner et al., 2019; Li et al., 2019). Analyzing lacustrine sediments from Lake Ohrid (Balkan Peninsula) Wagner et al. (2019) proposed that the Mediterranean winter precipitation varied in-phase with the African summer monsoon strength over glacial-interglacial cycles as both were driven by precessional and thus insolation forcing. The monsoon responded to rising summer insolation changes and Mediterranean precipitation to weakened winter insolation (Wagner et al., 2019; Cheng et al., 2016). Indeed, $\delta D_{wax\ n\text{-}alkanoic\ acid}$ and $\delta D_{wax\ n\text{-}alkanes}$ from core GeoB7702-3 confirm that Mediterranean winter rains and the African summer monsoon (Castañeda et al., 2016a; Costa et al., 2014, Berke et al., 2012, Tierney et al., 2008) were concurrently strong in the Nile River watershed during the AHP optimum but wet conditions began later (~11 ka BP) and also ended earlier (~6 ka BP) in the delta than in the upper river catchment (~14.5-5 ka BP; Figures 2a-d, 3d). The relatively short wet phase recorded in our

https://doi.org/10.5194/cp-2023-23
Preprint. Discussion started: 27 April 2023

$\delta D_{wax\ n\text{-alkanoic acid}}$ agrees with pronounced freshening of the northern Red Sea which has been interpreted to result from enhanced winter rainfall over Egypt and the Sinai Peninsula (Arz et al., 2003). Moreover, spring tufa deposits formed on the Sinai Peninsula only between 9.0-6.7 ka BP (Figure 3c) and were fed by Mediterranean moisture (Hamdan and Brook, 2015). Together these data show that in the northeastern Sahara wet conditions were restricted to the AHP optimum (11.0-6.5 ka BP) although winter insolation had already begun to decrease 7 ka earlier (Figure 3d,f). Likely, the storm track reached the northeastern Sahara only when the difference between summer insolation and winter insolation was maximal (Figures 3a,b,c,d). Interestingly, speleothem δ^{18}O-records from caves in Lebanon (Jeita Cave; Figure 1) suggest that the hydroclimate may have ameliorated slightly earlier, i.e. around 12 ka BP (Figure 3a,d) while Soreq Cave indicates an increase of humid conditions at the same time as $\delta D_{wax\ n\text{-alkanoic acid}}$ in core GeoB7702-3 (Figure 3b,d). The staggered onset of wet conditions in the south eastern Mediterranean realm may attest to the progressive southward migration of the storm track.

5.5.2 Implications for the "Green Sahara" (11-5 ka BP)

Providing insights into the development of summer and winter precipitation in the Nile-River watershed our findings are important for the understanding of the moisture sources which sustained the "Green Sahara". As elaborated by Castaneda et al. (2016), the $\delta D_{wax\ n\text{-alkane}}$ attest to enhanced monsoon rainfall in the Nile-River watershed. It is widely accepted that the northward migration and intensification of the summer monsoon was critical to trigger plant growth in the Sahara (Braconnot et al., 2007; Menviel et al., 2021; deMenocal et al., 2000b; Shannahan et al., 2015; Sha et al., 2019; Tierney et al., 2017). However, discrepancies between proxy data and climate simulations regarding precipitation and vegetation anomalies question that the monsoon was the only moisture source to the Sahara (Chandan et al., 2020; Braconnot et al., 2007; Hopcroft et al., 2017; Perez-Sanz et al., 2014; Cheddadi et al., 2021; Hély et al., 2014). Monsoonal precipitation may not have reached beyond ~24°N (Chandan et al., 2020; Braconnot et al., 2007; Hopcroft et al., 2017; Perez-Sanz et al., 2014) but vegetation extended up to 28-31°N (e.g. Hély et al., 2014; Tierney et al., 2017; Giraudi et al., 2013; Hamdan et al., 2016; Larrasoña et al., 2013). In the northern Sahara, south of the Nile Delta, the landscape turned into a semi-arid desert zone with covered by vegetation patches comprising open Savannah with mainly grasslands. Wetlands and trees likely flourished near permanent water bodies (Hamdan et al., 2016; Larrasoña et al., 2013). Some tropical plants migrated north of 25°N but were restricted along rivers and lakes (Hamdan et al., 2016; Larrasoña et al., 2013). Thus, with the monsoon extending up to 24°N, it likely was insufficient to support such vegetation in the northern Sahara. Our $\delta D_{wax\ n\text{-alkanoic acid}}$ show that Mediterranean winter rainfall enhanced when the Sahara became vegetated (Figure 3d). This suggests that winter rainfall provided additional moisture to the Northern Sahara. Our finding matches the results of Cheddadi et al. (2021) who proposed that Mediterranean winter rainfall played a crucial role in the genesis and sustaining of a green Sahara. Combining proxy data from Morocco with a vegetation model they show that intensified winter precipitation could have provided the additional moisture needed if the winter rainfall zone – which is restricted to a small area along the Mediterranean coast today – extended further south into the Sahara and perhaps even overlapped with the northward extended monsoon zone. The formation of the paleo Faiyum-Lake (Egypt, Figure 1) is dated to 10 ka BP (Hamdan et al., 2016; Hassan et al., 2012) and may give a first hint that also in the eastern Sahara winter

https://doi.org/10.5194/cp-2023-23
Preprint. Discussion started: 27 April 2023

rainfall increased south of the present-day limit of the Mediterranean rainfall zone (i.e. approximately the southern tip of the Nile delta, Cairo). However, the inundation of the Faiyum depression to a large extent is a result from high Nile floods which are linked to monsoonal rainfall and local precipitation is considered of minor importance (Hamdan et al., 2016; Hassan et al., 2012). Therefore, more supporting evidence for the southward extension of frequent winter rains during the AHP is needed. Seeking for indication that also in Northeast Africa the winter rainfall zone extended deeper into the Sahara the information should be potentially recorded in the $\delta D_{wax\ n\text{-alkane}}$ considering that HMW *n*-alkanes received substantial contributions from the upper and middle catchment while the HMW n-alkanoic acids derived mainly from the delta. Between 11-10 ka BP – at the onset of Saharan greening – the $\delta D_{wax\ n\text{-alkane}}$ shows a reversal to enriched δD values (Figure 3). The reversal to enriched $\delta D_{wax\ n\text{-alkane}}$ may either be interpreted as a reduction in rainfall amount or as a change in the moisture source. A similar reversal is not recorded in the δD_{wax} records from Lakes Tana, Victoria and Tanganyika (Berke et al., 2012, Tierney et al., 2008, Costa et al., 2014). These records even suggest that the monsoon strengthened at that time. Therefore, it is unlikely that the reversal in $\delta D_{wax\ n\text{-alkane}}$ between 11.5-10.5 ka BP stems from a weakened monsoon. Lake Tanganyika as well as other East African archives show that the monsoon weakened during the Younger Dryas (13.8-11.5 kaBP; Figure 2b,c; Tierney et al., 2008; Berke et al., 2014; Talbot et al., 2007). Castañeda et al. (2016) suggested the reversal would attest to drier conditions during Younger-Dryas stadial. However, we rule out that the enrichment in $\delta D_{wax\ n\text{-alkane}}$ is a delayed climate deterioration associated with the Younger Dryas considering our revised age model for core GeoB7702-3 (uncertainties: ~ ±360 yrs at 379 cm, Table 1). Given the absence of a comparable signal in the headwaters, the signal most likely was generated in the middle part of the Nile catchment, i.e. in the Sahara, south of the Nile delta. The reversal coincides with the beginning decrease of $\delta D_{wax\ n\text{-alkanoic acid}}$ and consequently with the starting intensification of winter precipitation at 11 ka BP (Figure 3). As such, the reversal to more enriched $\delta D_{wax\ n\text{-alkane}}$ between 11.5-10.5 ka BP probably attests to increased influence of Mediterranean precipitation in the Sahara. The general enrichment of $\delta D_{wax\ n\text{-alkanoic acid}}$ relative to $\delta D_{wax\ n\text{-alkane}}$ during the early AHP (~14.5-11 ka BP) provides evidence that the Mediterranean moisture was isotopically heavier than moisture from the Indian and Atlantic Oceans, the latter feeding the African summer monsoon (Figure 1). This further argues for Mediterranean influence on the $\delta D_{wax\ n\text{-alkane}}$ during this period. The minimum in $\delta D_{wax\ n\text{-alkane}}$ succeeding the reversal then probably also stems from the amplification of winter precipitation, given the strong similarity to the minimum in $\delta D_{wax\ n\text{-alkanoic acid}}$ which occurs concurrently (Figures 2, 3). This inference is supported by the absence of similar minima in δD_{wax} from Lakes Tana, Victoria and Tanganyika at that time (Berke et al., 2012, Costa et al., 2014, Tierney et al., 2008). Seeking to explain the minimum in $\delta D_{wax\ n\text{-alkane}}$ between 10 and 7 ka BP Castañeda et al. (2016a) invoked an eastward shift of the Congo Air Boundary during the AHP optimum which would enhance the influence of Atlantic moisture over the headwaters. However, the striking similarity between the $\delta D_{wax\ n\text{-alkane}}$ and $\delta D_{wax\ n\text{-alkanoic acid}}$ is a profound argument for the influence of winter precipitation. Acknowledging that $\delta D_{wax\ n\text{-alkane}}$ remain depleted relative to the $\delta D_{wax\ n\text{-alkanoic acid}}$ despite the influence of Mediterranean moisture (Figure 3), monsoon precipitation probably still substantially influenced the δDwax n-alkanes-signal. We conclude that during the peak phase of the AHP (11-6 ka BP), the $\delta D_{wax\ n\text{-alkanes}}$ record monsoonal precipitation superimposed by Mediterranean winter precipitation. As such, we deduce that the winter rainfall zone shifted southward during the AHP optimum. Our data confirm that the interplay of

https://doi.org/10.5194/cp-2023-23
Preprint. Discussion started: 27 April 2023

monsoon (summer) and Mediterranean (winter) may have provided the Sahara with sufficient rainfall throughout the year allowing for plants to occupy the nowadays barren desert (Cheddadi et al., 2021).

6. Conclusions

Analyzing $\delta D_{wax\ n\text{-alkanoic acid}}$ in core GeoB7702-3 from the Eastern Mediterranean we provide a continuous record for winter precipitation in the Nile-River delta for the past 18 ka BP, in a region where continuous records are sparse. By comparison to previously published records of $\delta D_{wax\ n\text{-alkanes}}$ from the same sediment core we gain new information about the provenance of leaf-wax lipids in the Nile River watershed and about the interplay of Mediterranean (winter) and monsoonal (summer) precipitation around the AHP and their significance for the genesis and sustaining of the Green Sahara. Our key findings can be summarized as follows:

1) HMW *n*-alkanoic acids predominantly derived from the delta during the past 18 ka while the source of the HMW *n*-alkanes varied through time as a function of river runoff and vegetation coverage in the Sahara. Between 15-4 ka BP the HMW *n*-alkanes received major contributions from the headwaters and the Sahara once the river runoff was relatively high due to intensified summer rains. Before and after this interval HMW *n*-alkanes derived from the delta region, like the HMW *n*-alkanoic acids. Around the AHP (14.5-5 ka BP) the paired application of $\delta D_{wax\ n\text{-alkanoic acids}}$ and $\delta D_{wax\ n\text{-alkane}}$ allows to reconstruct winter rainfall ($\delta D_{wax\ n\text{-alkanoic acid}}$) along with summer monsoonal precipitation ($\delta D_{wax\ n\text{-alkane}}$) in the Nile-River watershed

2) HS1 occurred in two phases in the Nile River delta due to rapid variations in the position of the westerly Jet and the associated storm track over the Mediterranean. First the climate became arid due to a northward shift of the storm track. At 16 ka BP wet conditions established as the storm track was pushed south. Afterwards the climate remained relatively dry until 11 ka BP as the westerly Jet moved north in response to ice sheet retreat.

3) In the Nile-delta we find evidence for increased Mediterranean winter rainfall between 11-6 ka BP corresponding the optimum of the AHP. Amplified winter precipitation resulted from a combination of local cyclogenesis promoted by elevated SSTs and southward displaced westerlies steering Atlantic storms into the Mediterranean. The episode of intensified rainfall was much shorter in the delta region than in the southern Nile catchment, where the summer monsoon determines precipitation. In the headwaters the hydroclimate has already begun to ameliorate as early as 14.5 ka BP. Likely, winter precipitation only increased when the storm track reached its southernmost position during maximal difference between NH summer and NH winter insolation.

4) At the time of Sahara greening and enhanced precipitation in the delta region (11-6 ka BP) the monsoonal signal in the $\delta D_{wax\ n\text{-alkane}}$ was superimposed by intensified Mediterranean precipitation in the Sahara. Given that we find proof for concurrently intensified winter and summer precipitation in the Nile-River watershed and infer that westerly precipitation was enhanced not only in the delta region but also penetrated farther south into the Sahara, our data support the recently raised hypothesis that monsoonal precipitation only together with winter precipitation could allow for vegetation to occupy the Sahara Desert.

Data availability

The data generated in this study will be accessible on the PANGAEA database https://www.pangaea.de/.

Competing interests

The authors declare that they have no conflict of interest.

Author contributions

ES designed the study together with VM, GM and JP. JP provided sediment material for core GeoB7702-3. VM carried out the sample and data processing. VM drafted the manuscript with contributions from all co-authors.

Acknowledgements

We thank the captain and the crew of RV Meteor for their effort during cruise M52/2. Pushpak Nadar is thanked for his valuable help during processing the biomarker and foraminifera samples in the laboratories at MARUM. Ralph Kreutz is acknowledged for his support during the isotope analysis. We thank Liz Bonk, Hendrik Grotheer and Torben Gentz for their efforts during the AMS measurements. This work was funded by the DFG Research Center/Excellence Cluster "The Ocean Floor – Earth's Uncharted Interface".

References

AbuBakr, M., Ghoneim, E., El-Baz, F., Zeneldin, M. and Zeid, S.: Use of radar data to unveil the paleolakes and the ancestral course of Wadi El-Arish, Sinai Peninsula, Egypt, Geomorphology, 194, 34–45, doi:10.1016/j.geomorph.2013.04.005, 2013.

Agrawal, S., Galy, V. V., Sanyal, P. and Eglinton, T. I.: C4 plant expansion in the Ganga Plain during the last glacial cycle: insights from isotopic composition of vascular plant biomarkers. Org. Geochem., 67, 58–71, doi:10.1016/j.orggeochem.2013.12.007, 2014.

Alpert, P., Baldi, M., Ilani, R., Krichak, S., Price, C., Rodó, X., Saaroni, H., Ziv, B., Kishcha, P., Barkan, J., Mariotti, A. and Xoplaki, E.: Relations between climate variability in the Mediterranean region and the tropics: ENSO, South Asian and African monsoons, hurricanes and Saharan dust, Dev. Earth Environ. Sci., 4, 149–177, doi:10.1016/S1571-9197(06)80005-4, 2006.

Arz, H., Lamy, F., Pätzold, J., Müller, P. and Prins, M. A.: Mediterranean moisture source for an Early-Holocene Humid Period in the Northern Red Sea, Science, 300, 118–121, doi:10.1126/science.1080325, 2003.

Bar-Matthews, M., Ayalon, A., Gilmour, M., Matthews, A. and Hawkesworth, C. J.: Sea - land oxygen isotopic relationships from planktonic foraminifera and speleothems in the Eastern Mediterranean region and their implication for paleorainfall during interglacial intervals, Geochim. Cosmochim. Acta, 67, 3181–3199, doi:10.1016/S0016-7037(02)01031-1, 2003.

Berger, A. and Loutre, M. F.: Insolation values for the climate of the last 10 million years, Quat. Sci. Rev., 10, 297–317, doi:10.1016/0277-3791(91)90033-Q, 1991.

Berke, M. A., Johnson, T. C., Werne, J. P., Grice, K., Schouten, S. and Sinninghe Damsté, J. S.: Molecular records of climate variability and vegetation response since the Late Pleistocene in the Lake Victoria basin, East Africa, Quat. Sci. Rev., 55, 59–74, doi:10.1016/j.quascirev.2012.08.014, 2012.

Berke, M. A., Johnson, T. C., Werne, J. P., Livingstone, D. A., Grice, K., Schouten, S. and Sinninghe Damsté, J. S.: Characterization of the last deglacial transition in tropical East Africa: Insights from Lake Albert, Palaeogeogr. Palaeoclimatol. Palaeoecol., 409, 1–8, doi:10.1016/j.palaeo.2014.04.014, 2014.

Blanchet, C. L., Contoux, C. and Leduc, G.: Runoff and precipitation dynamics in the Blue and White Nile catchments during the mid-Holocene: A data-model comparison, Quat. Sci. Rev., 130, 222–230, doi:10.1016/j.quascirev.2015.07.014, 2015.

Blanchet, C., Frank, M. and Schouten, S.: Asynchronous Changes in Vegetation, Runoff and Erosion in the Nile River Watershed during the Holocene, PLoS One, 9, 1–18, doi:10.1371/journal.pone.0115958, 2014.

Blanchet, C. L., Osborne, A. H., Tjallingii, R., Ehrmann, W., Friedrich, T., Timmermann, A., Brückmann, W. and Frank, M.: Drivers of river reactivation in North Africa during the last glacial cycle, Nat. Geosci., 14, 97-103, doi:10.1038/s41561-020-00671-3, 2021.

Blaauw, M. and Christen, A.: "Flexible paleoclimate age-depth models using an autoregressive gamma process." Bayesian Anal. 6, 457-474, doi:10.1214/11-BA618, 2011.

Bowen, G. J., Wassenaar, L. I. and Hobson, K. A.: Global application of stable hydrogen and oxygen isotopes to wildlife forensics, Oecologia, 143, 337–348, doi:10.1007/s00442-004-1813-y, 2005.

Braconnot, P., Otto-Bliesner, B., Harrison, S., Joussaume, S., Peterchmitt, J.-Y., Abe-Ouchi, A., Crucifix, M., Driesschaert, E., Fichefet, Th., Hewitt, C. D., Kageyama, M., Kitoh, A., Laîné, A., Loutre, M.-F., Marti, O., Merkel, U., Ramstein, G., Valdes, P., Weber, S. L., Yu, Y., and Zhao, Y.: Results of PMIP2 coupled simulations of the Mid-Holocene and Last Glacial Maximum – Part 1: experiments and large-scale features, Clim. Past, 3, 261–277, https://doi.org/10.5194/cp-3-261-2007, 2007

Breitenbach, S. F. M., Adkins, J. F., Meyer, H., Marwan, N., Kumar, K. K. and Haug, G. H.: Strong influence of water vapor source dynamics on stable isotopes in precipitation observed in Southern Meghalaya, NE India, Earth Planet. Sci. Lett., 292, 212–220, doi:10.1016/j.epsl.2010.01.038, 2010.

Camberlin, P.: Nile Basin Climates. In: The Nile. Springer, pp. 307–333, 2009.

Castañeda, I. S., Schefuß, E., Pätzold, J., Sinninghe Damsté, J. S., Weldeab, S. and Schouten, S.: Millennial-scale sea surface temperature changes in the eastern Mediterranean (Nile River Delta region) over the last 27,000 years, Paleoceanography, 25, 1–13, doi:10.1029/2009PA001740, 2010a.

Castañeda, I. S., Schefuß, E., Pätzold, J., Sinninghe Damsté., Weldeab, S. and Schouten, S.: (Table 1) Radiocarbon dating of sediment core GeoB7702-3. PANGAEA, doi:10.1594/PANGAEA.736913, 2010b.

Castañeda, I. S., Schefuß, E., Pätzold, J., Sinninghe Damsté., Weldeab, S. and Schouten, S.: Isoprenoidal GDGT and alkenone based proxies of sediment core GeoB7702-3. PANGAEA, doi:10.1594/PANGAEA.736909, 2010c.

https://doi.org/10.5194/cp-2023-23
Preprint. Discussion started: 27 April 2023

Castañeda, I. S., Schouten, S., Pätzold, J., Lucassen, F., Kasemann, S., Kuhlmann, H. and Schefuß, E.: Hydroclimate variability in the Nile River Basin during the past 28,000 years, Earth Planet. Sci. Lett., 438, 47–56, doi:10.1016/j.epsl.2015.12.014, 2016a.

Castañeda, I. S., Schouten, S., Pätzold, J., Lucassen, F., Kasemann, S. A., Kuhlmann, H., and Schefuß.: Organic geochemical analyses of sediment core GeoB7702-3, PANGAEA, doi.org:10.1594/PANGAEA.858559, 2016b

Chandan, D. and Peltier, W. R.: African humid period precipitation sustained by robust vegetation, soil, and Lake feedbacks. Geophys. Res. Lett, 47, e2020GL088728, doi:10.1029/2020GL088728, 2020.

Cheddadi, R., Carré, M., Nourelbait, M., François, L., Rhoujjati, A., Manay, R., Ochoa, D. and Schefuß, E.: Early Holocene greening of the Sahara requires Mediterranean winter rainfall, Proc. Natl. Acad. Sci., 118, e2024898118, doi:10.1073/pnas.2024898118, 2021.

Cheng, H., Sinha A., Verheyden, S., Nader, F. H., Li, X. L., Zhang, P. Z., Yin, J. J., Yi, L., Peng, Y. B., Rao, Z. G., Ning, Y. F. and Edwards, R. L.: The climate variability in northern Levant over the past 20,000 years, Geophys. Res. Lett., 42, 8641–8650, doi:10.1002/2015GL065397, 2015.

Cheng, H., Lawrence Edwards, R., Sinha, A., Spötl, C., Yi, L., Chen, S., Kelly, M., Kathayat, G., Wang, X., Li, X., Kong, X., Wang, Y., Ning, Y. and Zhang, H.: The Asian monsoon over the past 640,000 years and ice age terminations, Nature, 534, 640–646, https://doi.org/10.1038/nature18591, 2016.

Claussen, M., Dallmeyer, A. and Bader, J.: Theory and modeling of the African humid period and the green Sahara, in: Oxford Research Encyclopedia: Climate Science Vol. 1, Oxford Research Encyclopedia, Ed., Oxford University Press USA, 2017.

Collins, J. A., Schefuß, E., Mulitza, S., Prange, M., Werner, M., Tharammal, T., Paul, A. and Wefer, G.: Estimating the hydrogen isotopic composition of past precipitation using leaf-waxes from western Africa, Quat. Sci. Rev., 65, 88–101, doi:10.1016/j.quascirev.2013.01.007, 2013.

Collins, J. A., Prange, M., Caley, T., Gimeno, L., Beckmann, B., Mulitza, S., Skonieczny, C., Roche, D. and Schefuß, E.: Rapid termination of the African Humid Period triggered by northern high-latitude cooling, Nat. Commun., 8, doi:10.1038/s41467-017-01454-y, 2017.

Columbu, A., Spötl, C., Fohlmeister, J., Hu, H. M., Chiarini, V., Hellstrom, J., Cheng, H., Shen, C. C. and De Waele, J.: Central Mediterranean rainfall varied with high northern latitude temperatures during the last deglaciation, Commun. Earth Environ., 3, 1–9, doi:10.1038/s43247-022-00509-3, 2022.

Costa, K., Russell, J., Konecky, B. and Lamb, H.: Isotopic reconstruction of the African Humid Period and Congo Air Boundary migration at Lake Tana, Ethiopia, Quat. Sci. Rev., 83, 58–67, doi:10.1016/j.quascirev.2013.10.031, 2014.

De Jonge, C., Stadnitskaia, A., Hopmans, E. C., Cherkashov, G., Fedotov, A. and Sinninghe Damsté, J. S.: In situ produced branched glycerol dialkyl glycerol tetraethers in suspended particulate matter from the Yenisei River, Eastern Siberia, Geochim. Cosmochim. Acta, 125, 476–491, doi:10.1016/j.gca.2013.10.031, 2014.

deMenocal, P. B.: Palaeoclimate: End of the African humid period, Nat. Geosci., 8, 86–87, doi:10.1038/ngeo2355, 2015.

deMenocal, P., Ortiz, J., Guilderson, T., Adkins, J., Sarnthein, M., Baker, L. and Yarusinsky, M.: Abrupt onset and termination of the African Humid Period: rapid climate responses to gradual insolation forcing, Quat. Sci. Rev., 19, 347–361, doi:10.1016/S0277-3791(99)00081-5, 2000a.

deMenocal P., Ortiz J., Guilderson T. and Sarnthein M.: Coherent high- and low-latitude climate variability during the Holocene warm period, Science, 288, 2198–2202, doi: 10.1126/science.288.5474.2198, 2000b.

Dixit, Y., Toucanne, S., Fontanier, C., Pasquier, V., Lora, J. M., Jouet, G. and Tripati, A.: Enhanced western Mediterranean rainfall during past interglacials driven by North Atlantic pressure changes, Quat. Int., 553, 1–13, doi:10.1016/j.quaint.2020.08.017, 2020.

Eglinton, T. I. and Eglinton, G.: Molecular proxies for paleoclimatology, Earth Planet. Sci. Lett., 275, 1–16, doi:10.1016/j.epsl.2008.07.012, 2008.

Eglinton, G. and Hamilton, R. J.: Leaf epicuticular waxes, Science, 156, 1322–1335, doi: 10.1126/science.156.3780.1322, 1967.

Emeis, K. C., Struck, U., Schulz, H. M., Rosenberg, R., Bernasconi, S., Erlenkeuser, H., Sakamoto, T. and Martinez-Ruiz, F.: Temperature and salinity variations of Mediterranean Sea surface waters over the last 16,000 years from records of planktonic stable oxygen isotopes and alkenone unsaturation ratios, Palaeogeogr. Palaeoclimatol. Palaeoecol., 158, 259–280, doi:10.1016/S0031-0182(00)00053-5, 2000.

Fletcher, W. J., Goni, M. F. S., Peyron, O. and Dormoy, I.: Abrupt climate changes of the last deglaciation detected in a Western Mediterranean forest record, Clim. Past, 6, 245–264, doi:10.5194/cp-6-245-2010, 2010.

Fletcher, W. J. and Sanchez Goñi, M. F.: Orbital- and sub-orbital-scale climate impacts on vegetation of the western Mediterranean basin over the last 48,000 yr. Quat. Res., 70, 451-464, doi:10.1016/j.yqres.2008.07.002, 2008.

Galy, V. and Eglinton, T.: Protracted storage of biospheric carbon in the Ganges-Brahmaputra basin, Nat. Geosci., 4, 843–847, doi:10.1038/ngeo1293, 2011.

Garcin, Y., Schefuß, E., Schwab, V. F., Garreta, V., Gleixner, G., Vincens, A., Todou, G., Séné, O., Onana, J. M., Achoundong, G. and Sachse, D.: Reconstructing C3 and C4 vegetation cover using n-alkane carbon isotope ratios in recent lake sediments from Cameroon, Western Central Africa, Geochim. Cosmochim. Acta, 142, 482–500, doi:10.1016/j.gca.2014.07.004, 2014.

Giraudi, C., Mercuri, A. M. and Esu, D.: Holocene palaeoclimate in the northern Sahara margin (Jefara Plain, northwestern Libya), The Holocene, 23, 339–352, doi:10.1177/0959683612460787, 2013.

Häggi, C., Sawakuchi, A. O., Chiessi, C. M., Mulitza, S., Mollenhauer, G., Sawakuchi, H. O., Baker, P. A., Zabel, M. and Schefuß, E.: Origin, transport and deposition of leaf-wax biomarkers in the Amazon Basin and the adjacent Atlantic, Geochim. Cosmochim. Acta, 192, 149–165, doi:10.1016/j.gca.2016.07.002, 2016.

Hamdan, M. A. and Brook, G. A.: Timing and characteristics of Late Pleistocene and Holocene wetter periods in the Eastern Desert and Sinai of Egypt, based on 14C dating and stable isotope analysis of spring tufa deposits, Quat. Sci. Rev., 130, 168–188, doi:10.1016/j.quascirev.2015.09.011, 2015.

Hamdan, M. A., Ibrahim, M. I. A., Shiha, M. A., Flower, R. J., Hassan, F. A. and Eltelet, S. A. M.: An exploratory Early and Middle Holocene sedimentary record with palynoforms and diatoms from Faiyum lake, Egypt, Quat. Int., 410, 30–42, doi:10.1016/j.quaint.2015.12.049, 2016.

Hamdan, M.A. and Lucarini, G.: Holocene paleoenvironmental, paleoclimatic and geoarchaeological significance of the Sheikh El-Obeiyid area (Farafra Oasis, Egypt), Quat. Int., 302, 154-168, doi:10.1016/j.quaint.2013.01.009, 2013.

Hassan, F. A., Hamdan, M. A., Flower, R. J. and Keatings, K.: Oxygen and carbon isotopic records in Holocene freshwater mollusc shells from the Faiyum palaeolakes, Egypt: Palaeoenvironmental and palaeoclimatic implications, Quat. Int., 266, 175–187, doi:10.1016/j.quaint.2011.11.024, 2012.

Heaton, T. J., Köhler, P., Butzin, M., Bard, E., Reimer, R. W., Austin, W. E. N., Bronk Ramsey, C., Grootes, P. M., Hughen, K. A., Kromer, B., Reimer, P. J., Adkins, J., Burke, A., Cook, M. S., Olsen, J. and Skinner, L. C.: Marine20—The Marine Radiocarbon Age Calibration Curve (0–55,000 cal. BP), Radiocarbon, 62: IntCal20: Calibration Issue, 779–820, doi:10.1017/RDC.2020.68, 2020.

Hély, C., Lézine, A. M., Ballouche, A., Cour, P., Duzer, D., Guinet, P., Jahns, S., Maley, J., Mercuri, A. M., Pons, A., Ritchie, J. C., Salzmann, U., Schulz, E., Van Campo, M. and Waller, M. P.: Holocene changes in African vegetation: Tradeoff between climate and water availability, Clim. Past, 10, 681–686, doi:10.5194/cp-10-681-2014, 2014.

Hemingway, J. D., Schefuß, E., Dinga, B. J., Pryer, H. and Galy, V. V.: Multiple plant-wax compounds record differential sources and ecosystem structure in large river catchments, Geochim. Cosmochim. Acta, 184, 20–40, doi:10.1016/j.gca.2016.04.003, 2016.

Hoefs, M. J. L., Rijpistra, W. I. C. and Sinninghe Damste, J.S.: The influence of oxic degradation on the sedimentary biomarker record I: evidence from Madeira Abyssal Plain turbidites. Geochim. Cosmochim. Acta, 66, 2719–2735, doi:10.1016/S0016-7037(02)00864-5, 2002.

Hopcroft, P. O., Valdes, P. J., Harper, A., B. and Beerling, D. J.: Multi vegetation model evaluation of the green Sahara climate regime, Geophys. Res. Lett., 44, 6804–6813, doi:10.1002/2017GL073740, 2017.

https://en.climate-data.org/africa/egypt/cairo-governorate/cairo-3392/; (checked December, 14th 2022)

https://en.climate-data.org/africa/egypt/alexandria-governorate/alexandria-515/ (checked December, 14th 2022)

https://en.climate-data.org/africa/egypt/luxor-governate/luxor-6345/ (checked December, 14th 2022)

https://en.climate-data.org/africa/ethiopia/addis-ababa/addis-abeba-532/ (checked December, 14th 2022)

https://en.climate-data.org/africa/uganda/central-region/kampala-5578/ (checked December, 14th 2022)

Jolly, D., Prentice, I. C., Bonnefille, R., Ballouche, A., Bengo, M., Brenac, P., Buchet, G., Burney, D., Cazet, J. P., Cheddadi, R., Edorh, T., Elenga, H., Elmoutaki, S., Guiot, J., Laarif, F., Lamb, H., Lezine, A. M., Maley, J., Mbenza, M., Peyron, O., Reille, M., Reynaud-Farrera, I., Riollet, G., Ritchie, J. C., Roche, E., Scott, L., Ssemmanda, I., Straka, H., Umer, M., Van Campo, E., Vilimumbalo, S., Vincens, A. and Waller, M.: Biome reconstruction from pollen and plant macrofossil data for Africa and the Arabian peninsula at 0 and 6000 years, J. Biogeogr., 25, 1007–1027, doi:10.1046/j.1365-2699.1998.00238.x, 1998.

https://doi.org/10.5194/cp-2023-23
Preprint. Discussion started: 27 April 2023

Climate of the Past Discussions

Junginger, A., Roller, S., Olaka, L. A. and Trauth, M. H.: The effects of solar irradiation changes on the migration of the Congo Air Boundary and water levels of paleo-Lake Suguta, Northern Kenya Rift, during the African Humid Period (15–5 ka BP), Palaeogeogr. Palaeoclimatol. Palaeoecol., 396, 1–16., doi:10.1016/j.palaeo.2013.12.007, 2014.

Korecha, D. and Barnston, A.G.: Predictability of June–September Rainfall in Ethiopia. Mon. Wea. Rev., 135, 628–650, doi:10.1175/MWR3304.1, 2007

Kuper, R. and Kröpelin, S.: Climate-controlled Holocene occupation in the Sahara: Motor of Africa's evolution, Science, 313, 803–807, doi:10.1126/science.1130989, 2006.

Kutzbach, J. E., Chen, G., Cheng, H., Edwards, R. L. and Liu, Z.: Potential role of winter rainfall in explaining increased moisture in the Mediterranean and Middle East during periods of maximum orbitally-forced insolation seasonality, Clim. Dyn., 42, 1079–1095, doi:10.1007/s00382-013-1692-1, 2014.

Lamb, H. F., Bates, C. R., Coombes, P. V., Marshall, M. H., Umer, M., Davies, S. J. and Dejen, E.: Late Pleistocene desiccation of Lake Tana, source of the Blue Nile, Quat. Sci. Rev., 26, 287–299, doi:10.1016/j.quascirev.2006.11.020, 2007.

Larrasoaña, J. C., Roberts, A. P. and Rohling, E. J.: Dynamics of Green Sahara Periods and Their Role in Hominin Evolution, PLoS One, 8, e76514, doi:10.1371/journal.pone.0076514, 2013.

Li, Y., Song, Y., Yin, Q., Han, L. and Wang, Y.: Orbital and millennial northern mid-latitude westerlies over the last glacial period, Clim. Dyn., 53, 3315–3324, doi:10.1007/s00382-019-04704-5, 2019.

Lisiecki, L. E., and Raymo, M. E.: A Pliocene-Pleistocene stack of 57 globally distributed benthic δ18O records, Paleoceanography, 20, PA1003, doi:10.1029/2004PA001071, 2005.

Lüning, S. and Vahrenholt, F.: Holocene Climate Development of North Africa and the Arabian Peninsula, in: Bendaoud, A., Hamimi, Z., Hamoudi, M., Djemai, S. and Zoheir, B.: The Geology of the Arab World - An Overview, pp. 507-546, Springer Geology, 2019, https://doi.org/10.1007/978-3-319-96794-3

Martin, C., Ménot, G., Thouveny, N., Davtian, N., Andrieu-Ponel, V., Reille, M. and Bard, E.: Impact of human activities and vegetation changes on the tetraether sources in Lake St Front (Massif Central, France), Org. Geochem., 135, 38–52, doi:10.1016/j.orggeochem.2019.06.005, 2019

Marshall, M.H., Lamb, H.F., Huws, D., Davies, S.J., Bates, R., Bloemendal, J., Boyle, J., Leng, M.J., Umer, M. and Bryant, C.: Late Pleistocene and Holocene drought events at Lake Tana, the source of the Blue Nile, Glob. Planet. Change, 78, 147–161, doi:10.1016/j.gloplacha.2011.06.004, 2011.

Meyers, P. A. and Ishiwatari, R.: Lacustrine organic geochemistry – an overview of indicators of organic matter sources and diagenesis in lake sediments, Org. Geochem., 20, 867–900, doi:10.1016/0146-6380(93)90100-P, 1993.

Ménot, G., Pivot, S., Bouloubassi, I., Davtian, N., Hennekam, R., Bosch, D., Ducassou, E., Bard, E., Migeon, S. and Revel, M.: Timing and stepwise transitions of the African Humid Period from geochemical proxies in the Nile deep-sea fan sediments, Quat. Sci. Rev., 228, doi:10.1016/j.quascirev.2019.106071, 2020.

Menviel, L., Govin, A. and Grant, K. M.: Drivers of the evolution and amplitude of African Humid Periods, Commun. Earth Environ., 2, 237, doi:10.1038/s43247-021-00309-1, 2021.

Mollenhauer, G., Grotheer, H., Gentz, T., Bonk, E. and Hefter, J.: Standard operation procedures and performance of the MICADAS radiocarbon laboratory at Alfred Wegener Institute (AWI), Germany, Nucl. Instruments Methods Phys. Res. Sect. B Beam Interact. with Mater. Atoms, 496, 45–51, doi:10.1016/j.nimb.2021.03.016, 2021.

Muhs, D. R., Roskin, J., Tsoar, H., Skipp, G., Budahn, J. R., Sneh, A., Porat, N., Stanley, J. D., Katra, I. and Blumberg, D. G.: Origin of the Sinai-Negev erg, Egypt and Israel: Mineralogical and geochemical evidence for the importance of the Nile and sea level history, Quat. Sci. Rev., 69, 28–48, doi:10.1016/j.quascirev.2013.02.022, 2013.

Naughton, F., Sánchez Goñi, M.F., Kageyama, M., Bard, E., Cortijo, E., Desprat, S., Malaizé, B., Joly, C., Rostek, F. and Turon, J.-L.: Wet to dry climatic trend in north western Iberia within Heinrich events, Earth Planet. Sci. Let., 284, 329-342, doi:10.1016/j.epsl.2009.05.001, 2009.

Naughton, F., Sanchez Goñi, M.F., Rodrigues, T., Salgueiro, E., Costas, S., Desprat, S., Duprat, J., Michel, E., Rossignol, L., Zaragosi, S., Voelker, A. H. L. and Abrantes, F.: Climate variability across the last deglaciation in NW Iberia and its margin, Quat. Int., 414, 9-22, doi:10.1016/j.quaint.2015.08.073, 2016.

Naughton, F., Toucanne, S., Landais, A., Rodrigues, T., Vazquez Riveiros, N. and Sánchez-Goñi, M. F.: Chapter 5 – Heinrich Stadial 1. In: Palacios, D., Hughes, P. D., García-Ruiz, J. M. and Andrés N.: European Glacial Landscapes – The Last Deglaciation, Elsivier, 37-44, ISBN 9780323918992, doi.org/10.1016/B978-0-323-91899-2.00049-8, 2023.

Otto-Bliesner, B. L., Russell, J. M., Clark, P. U., Liu, Z., Overpeck, J. T., Konecky, B., Nicholson, S. E., He, F. and Lu, Z.: Coherent changes of southeastern equatorial and northern African rainfall during the last deglaciation, Science, 346, 1223–1227, doi:10.1126/science.1259531, 2014.

Pausata, F. S. R., Messori, G. and Zhang, Q.: Impacts of dust reduction on the northward expansion of the African monsoon during the green Sahara period, Earth Planet. Sci. Lett., 434, 298–307, doi:10.1016/j.epsl.2015.11.049, 2016.

Pausata, F. S. et al.: The greening of the Sahara: Past changes and future implications. One Earth 2, 235–250, doi:10.1016/j.oneear.2020.03.002,2020.

Pätzold, J., Bohrmann, G. and Hübscher, C.: Black Sea – Mediterranean – Red Sea. Cruise No. 52, January 2 – March 27, 2002, Istanbul – Limassol, Universität Hamburg, METEOR-Berichte 3-2, 178 pp, 2003.

Pérez-Mejías, C., Moreno, A., Bernal-Wormull, J., Cacho, I., Osácar, M.C., Lawrence, E. and Chang, E.: Oldest Dryas hydroclimate reorganization in the eastern Iberian Peninsula after the iceberg discharges of Heinrich Event 1, Quat. Res., 101, 67-83, doi:10.1017/qua.2020.112, 2021.

Perez-Sanz, A., Li, G., González-Sampériz, P., and Harrison, S. P.: Evaluation of modern and mid-Holocene seasonal precipitation of the Mediterranean and northern Africa in the CMIP5 simulations, Clim. Past, 10, 551–568, https://doi.org/10.5194/cp-10-551-2014, 2014.

Quade, J., Dente, E., Armon, M., Ben Dor, Y., Morin, E., Adam, O. and Enzel, Y.: Megalakes in the Sahara? A Review, Quat. Res., 90, 253–275, doi:10.1017/qua.2018.46, 2018.

Reimer, P. J. and Reimer, R. W.: A marine reservoir correction database and on-line interface. Radiocarbon, 43,461-3, doi:10.1017/S0033822200038339, 2001.

Revel, M., Ducassou, E., Grousset, F. E., Bernasconi, S. M., Migeon, S., Revillon, S., Mascle, J., Murat, A., Zaragosi, S. and Bosch, D.: 100,000 Years of African monsoon variability recorded in sediments of the Nile margin, Quat. Sci. Rev., 29, 1342–1362, doi:10.1016/j.quascirev.2010.02.006, 2010.

Revel, M., Colin, C., Bernasconi, S., Combourieu-Nebout, N., Ducassou, E., Grousset, F. E., Rolland, Y., Migeon, S., Bosch, D., Brunet, P., Zhao, Y. and Mascle, J.: 21,000 years of Ethiopian African monsoon variability recorded in sediments of the western Nile deep-sea fan, Reg. Environ. Chang., 14, 1685–1696, doi:10.1007/s10113-014-0588-x, 2014.

Revel, M., Ducassou, E., Skonieczny, C., Colin, C., Bastian, L., Bosch, D., Migeon, S. and Mascle, J.: 20,000 years of Nile River dynamics and environmental changes in the Nile catchment area as inferred from Nile upper continental slope sediments, Quat. Sci. Rev., 130, 200–221, doi:10.1016/j.quascirev.2015.10.030, 2015.

Sachse, D., Billault, I., Bowen, G. J., Chikaraishi, Y., Dawson, T. E., Feakins, S. J., Freeman, K. H., Magill, C. R., McInerney, F. A., van der Meer, M. T. J., Polissar, P., Robins, R. J., Sachs, J. P., Schmidt, H.-L., Sessions, A. L., White, J. W. C., West, J. B. and Kahmen, A.: Molecular paleohydrology: interpreting the hydrogen-isotopic composition of lipid biomarkers from photosynthesizing organisms, Annu. Rev. Earth Planet. Sci., 40, 221–249, doi:10.1146/annurev-earth-042711-105535, 2012.

Schefuß, E., Kuhlmann, H., Mollenhauer, G., Prange, M. and Pätzold, J.: Forcing of wet phases in southeast Africa over the past 17,000 years, Nature, 480, 509–512, doi:10.1038/nature10685, 2011.

Schefuß, E., Schouten, S. and Schneider, R. R.: Climatic controls on central African hydrology during the past 20,000 years. Nature, 437, 1003–1006, doi:10.1038/nature03945, 2005.

Schlitzer, R. Ocean Data View v.5.6.3 (Alfred Wegener Institute, 2006); https://odv.awi.de/

Sha, L., Ait Brahim, Y., Wassenburg, J. A., Yin, J., Peros, M., Cruz, F. W., Cai, Y., Li, H., Du, W., Zhang, H., Edwards, R. L. and Cheng, H.: How Far North Did the African Monsoon Fringe Expand During the African Humid Period? Insights From Southwest Moroccan Speleothems, Geophys. Res. Lett., 46, 14093–14102, doi:10.1029/2019GL084879, 2019.

Shanahan, T. M., Mckay, N. P., Hughen, K. A., Overpeck, J. T., Otto-Bliesner, B., Heil, C. W., King, J., Scholz, C. A. and Peck, J.: The time-transgressive termination of the African humid period, Nat. Geosci., 8, 140–144, doi:10.1038/ngeo2329, 2015.

Sinninghe Damsté, J. S., Rijpistra, W. I. C. and Reichart, G.-J.: The influence of oxic degradation on the sedimentary biomarker record II. Evidence from Arabian Sea sediments, Geochim. Cosmochim. Acta, 66, 2737–2754, doi:10.1016/S0016-7037(02)00865-7, 2002.

Stager, J. C., Ryves, D. B., Chase, B. M. and Pausata, F. S.: Catastrophic drought in the Afro-Asian monsoon region during Heinrich event 1. Science, 331, 1299–1302, doi:10.1126/science.1198322, 2011.

Talbot, M. R., Filippi, M. L., Jensen, N. B. and Tiercelin, J. J.: An abrupt change in the African monsoon at the end of the Younger Dryas, Geochemistry, Geophys. Geosystems, 8, Q03006, doi:10.1029/2006GC001465, 2007.

Tierney, J. E., Russell, J. M., Huang, Y., Sinninghe Damsté, J. S., Hopmans, E. C. and Cohen, A. S.: Northern hemisphere controls on tropical southeast African climate during the past 60,000 years, Science, 322, 252–255, doi:10.1126/science.1160485, 2008.

Tierney, J. E., Russell, J. M. and Huang, Y.: A molecular perspective on Late Quaternary climate and vegetation change in the Lake Tanganyika basin, East Africa, Quat. Sci. Rev., 29, 787–800, doi:10.1016/j.quascirev.2009.11.030, 2010.

Tierney, J. E., deMenocal, P. B.: Abrupt shifts in Horn of Africa hydroclimate since the Last Glacial Maximum. Science, 342, 843–846, doi:10.1126/science.1240411, 2013.

Tierney, J. E., Pausata, F. S. R. and deMenocal, P. B.: Rainfall regimes of the Green Sahara, Sci. Adv., 3, 1–10, doi:10.1126/sciadv.1601503, 2017.

Valsecchi, V., Sanchez Goñi, M. F. and Londeix, L.: Vegetation dynamics in the Northeastern Mediterranean region during the past 23 000 yr: Insights from a new pollen record from the Sea of Marmara, Clim. Past, 8, 1941–1956, doi:10.5194/cp-8-1941-2012, 2012.

Viste, E. and Sorteberg, A.: The effect of moisture transport variability on Ethiopian summer precipitation, Int. J. Climatol, 33, 3106–3123, doi:10.1002/joc.3566, 2013.

Wagner, B., Vogel, H., Francke, A., Friedrich, T., Donders, T., Lacey, J. H., Leng, M. J., Regattieri, E., Sadori, L., Wilke, T., Zanchetta, G., Albrecht, C., Bertini, A., Combourieu-Nebout, N., Cvetkoska, A., Giaccio, B., Grazhdani, A., Hauffe, T., Holtvoeth, J., Joannin, S., Jovanovska, E., Just, J., Kouli, K., Kousis, I., Koutsodendris, A., Krastel, S., Lagos, M., Leicher, N., Levkov, Z., Lindhorst, K., Masi, A., Melles, M., Mercuri, A. M., Nomade, S., Nowaczyk, N., Panagiotopoulos, K., Peyron, O., Reed, J. M., Sagnotti, L., Sinopoli, G., Stelbrink, B., Sulpizio, R., Timmermann, A., Tofilovska, S., Torri, P., Wagner-Cremer, F., Wonik, T. and Zhang, X.: Mediterranean winter rainfall in phase with African monsoons during the past 1.36 million years, Nature, 573, 256–260, doi:10.1038/s41586-019-1529-0, 2019.

Wang, N., Jiang, D. and Lang, X.: Northern westerlies during the last glacial maximum: Results from CMIP5 simulations, J. Clim., 31, 1135–1153, doi:10.1175/JCLI-D-17-0314.1, 2018.

Wassenburg, J. A., Dietrich, S., Fietzke, J., Fohlmeister, J., Jochum, K. P., Scholz, D., Richter, D. K., Sabaoui, A., Spötl, C., Lohmann, G., Andreae, M. O. and Immenhauser, A.: Reorganization of the North Atlantic Oscillation during early Holocene deglaciation, Nat. Geosci., 9, 602–605, doi:10.1038/ngeo2767, 2016.

Weldeab, S., Emeis, K.-C., Hemleben, C. and Siebel, W.: Provenance of lithogenic surface sediments and pathways of riverine suspended matter in the Eastern Mediterranean Sea: evidence from 143Nd/144Nd and 87Sr/86Sr ratios. Chem. Geol. 186, 139–149, doi:10.1016/S0009-2541(01)00415-6, 2002.

Weldeab, S., Menke, V. and Schmiedl, G: The pace of East African monsoon evolution during the Holocene, Geophys. Res. Lett., 41, 1724–1732, doi:10.1002/2014GL059361, 2014.

Weijers, J. W. H., Schouten, S., Hopmans, E. C., Geenevasen, J. A. J., David, O. R. P., Coleman, J. M., Pancost, R. D., Sinninghe Damsté, J. S.: Membrane lipids of mesophilic anaerobic bacteria thriving in peats have typical archaeal traits, Environ. Microbiol., 8, 648–657, doi:10.1111/j.1462-2920.2005.00941.x, 2006.

Williams, M., Talbot, M., Aharon, P., Abdl Salaam, Y., Williams, F. and Inge Brendeland, K.: Abrupt return of the summer monsoon 15,000 years ago: new supporting evidence from the lower White Nile valley and Lake Albert. Quat. Sci. Rev. 25, 2651–2665, doi:10.1016/j.quascirev.2005.07.019, 2006.

Zaki, A. S., King, G. E., Haghipour, N., Giegengack, R., Watkins, S. E., Gupta, S., Schuster, M., Khairy, H., Ahmed, S., El-Wakil, M., Eltayeb, S. A., Herman, F. and Castelltort, S.: Did increased flooding during the African Humid Period force migration of modern humans from the Nile Valley?, Quat. Sci. Rev., 272, doi:10.1016/j.quascirev.2021.107200, 2021.